AFOSR-TR- 87-1633

RF Project 764977/717636
Annual Report

STRENGTH AND STRUCTURE OF $Ga_{1-x}In_xAs$ ALLOYS

Sponsored by

ADVANCED RESEARCH PROJECTS AGENCY (DoD)

ARPA Order No. 5526

Monitored by AFOSR Under Contract #F49620-85-C-0129

Principal Investigator:
Katherine T. Faber
(614) 292-6725

Co-Principal Investigator:
John P. Hirth
(614) 292-0176

Program Manager:
Captain Kevin Malloy
(202) 767-4984

September 30, 1987

OSU

The Ohio State University Research Foundation
1314 Kinnear Road
Columbus, Ohio 43212

UNCLASSIFIED
SECURITY CLASSIFICATION OF THIS PAGE

REPORT DOCUMENTATION PAGE

Form Approved
OMB No. 0704-0188

1a. REPORT SECURITY CLASSIFICATION
Unclassified

1b. RESTRICTIVE MARKINGS

2a. SECURITY CLASSIFICATION AUTHORITY

3. DISTRIBUTION / AVAILABILITY OF REPORT
Approved for public release; distribution unlimited.

2b. DECLASSIFICATION / DOWNGRADING SCHEDULE

4. PERFORMING ORGANIZATION REPORT NUMBER(S)
764977/717636

5. MONITORING ORGANIZATION REPORT NUMBER(S)
AFOSR-TR- 87-1633

6a. NAME OF PERFORMING ORGANIZATION
The Ohio State University Research Foundation

6b. OFFICE SYMBOL (If applicable)

7a. NAME OF MONITORING ORGANIZATION
AFOSR

6c. ADDRESS (City, State, and ZIP Code)
1314 Kinnear Road
Columbus, OH 43212

7b. ADDRESS (City, State, and ZIP Code)
Department of the Air Force
Bolling AFB, DC 20332-6448

8a. NAME OF FUNDING / SPONSORING ORGANIZATION
AFOSR

8b. OFFICE SYMBOL (If applicable)
NE

9. PROCUREMENT INSTRUMENT IDENTIFICATION NUMBER
Contract No. F49620-85-C-0129

8c. ADDRESS (City, State, and ZIP Code)
Same as 7b

10. SOURCE OF FUNDING NUMBERS

PROGRAM ELEMENT NO.	PROJECT NO.	TASK NO.	WORK UNIT ACCESSION NO.
61102F	2917	A3	

11. TITLE (Include Security Classification)
Strength and Structure of $Ga_{1-x}In_xAs$ Alloys

12. PERSONAL AUTHOR(S)
Katherine T. Faber and John Hirth

13a. TYPE OF REPORT	13b. TIME COVERED	14. DATE OF REPORT (Year, Month, Day)	15. PAGE COUNT
Annual	FROM 9-1-86 TO 8-31-87	September 30, 1987	43

16. SUPPLEMENTARY NOTATION

17. COSATI CODES		
FIELD	GROUP	SUB-GROUP

18. SUBJECT TERMS (Continue on reverse if necessary and identify by block number)
10 to the 20th, cc, .0001

19. ABSTRACT (Continue on reverse if necessary and identify by block number)

Solid solution strengthening of GaAs by In atoms acting as $InAs_4$ units has been predicted for an intermediate temperature, plateau region. This strengthening could partially account for the reduction in dislocation density in crystals grown from the melt. Deformation studies of undoped and In-doped ($1\text{-}2\times10^{20}$ atoms.cm^{-3}) GaAs were performed in compression in the temperature range 500 - 1100°C at a strain rate of $10^{-4}s^{-1}$ in both multiple slip, [001], and single slip, [123], orientations. The critical resolved shear stress is nearly doubled with indium additions, but both undoped and In-doped materials show a weakly temperature independent critical resolved shear stress, expected from the solid solution strengthening model. The results also showed that the onset of dynamic recovery occurred at higher stress and strain levels for the In-doped materials, suggesting that the climb process is more difficult in these alloys. Transmission (cont.)

20. DISTRIBUTION / AVAILABILITY OF ABSTRACT
☐ UNCLASSIFIED/UNLIMITED ☒ SAME AS RPT. ☐ DTIC USERS

21. ABSTRACT SECURITY CLASSIFICATION
Unclassified

22a. NAME OF RESPONSIBLE INDIVIDUAL
Captain Kevin Malloy

22b. TELEPHONE (Include Area Code)
202-767-4933

22c. OFFICE SYMBOL
Electronic & Mat. Sci. NE

DD Form 1473, JUN 86 *Previous editions are obsolete.*

SECURITY CLASSIFICATION OF THIS PAGE
UNCLASSIFIED

19. (cont.)

electron microscopy substantiated these results. Additional studies are underway on II-VI compounds ($Cd_{1-x}Mn_xTe$) which may also demonstrate solid solution strengthening.

STRENGTH AND STRUCTURE OF $Ga_{1-x}In_xAs$ ALLOYS

Sponsored by

Advanced Research Projects Agency (DoD)

ARPA Order No. 5526

Monitored by AFOSR Under Contract #F49620-85-C-0129

Principal Investigator:
Katherine T. Faber
(614) 292-6725

Co-Principal Investigator:
John P. Hirth
(614) 292-0176

Program Manager:
Captain Kevin Malloy
(202) 767-4984

September 30, 1987

Report Summary

A. Technical Problem

In recent years it has been noted that small additions of indium (on the order of 1 atomic %) to gallium arsenide grown from the melt greatly reduces the dislocation density to less than $10^2 cm^{-2}$. The mechanism by which this phenomenon occurs has been speculated to be solid solution strengthening, in which In together with its four nearest neighbor As atoms acts as the hardening unit. In order to verify this strengthening mechanism, a program has been undertaken to determine the strength of $Ga_{1-x}In_xAs$ alloys as a function of temperature and composition. In the first year of the study, Vickers hardness measurements as a function of temperature were used as a preliminary assessment of solid solution strengthening, since microhardness is a good first cut to examine if materials exhibit a plateau stress associated with solid solution strengthening. These experiments required construction of a hardness tester described in an earlier report. This second year of study, consisting of compression tests and transmission electron microscopy, will be described herein. In addition to work on III-V system, it is of interest to pursue similar studies in II-VI compounds which potentially demonstrate enhanced mechanical properties by the addition of isoelectronic elements. Preliminary studies on the II-VI compound $Cd_{1-x}Mn_xTe$ will also be described.

B. General Methodology

The experiments used to study solid solution strengthening in the second phase of this work are uniaxial compression tests. Compression testing of undoped GaAs and GaAs containing $1\text{-}2x10^{20}$ atoms$\cdot cm^{-3}$ of In were carried out at temperatures of 500, 700, 900, 1000 and 1100°C at a strain

rate of $10^{-4}s^{-1}$ in the [001] orientation favoring the operation of multiple slip systems and in the [123] orientation favoring a single slip system.

Compression testing as a function of temperature in single slip and multiple slip orientations were used to determine the critical resolved shear stress (CRSS) directly from the stress strain curve. In these tests, the specimen surface is protected in a bath of B_2O_3 to prevent As volatilization and this allows tests to be performed at temperatures near the melting point. These tests are more difficult to conduct than hardness tests but supersede the problem of surface degradation present in the hot hardness tests at elevated temperatures.

Additional work on strain rate dependence has been carried out on a limited basis. Stress relaxation measurements were made following compression tests in the [001] orientation at 700, 900 and 1100°C. Because significant microyielding is expected at stresses below the yield point at these high temperatures, it is important to look at the dislocation structure development as a function of stress level, mostly around the macroscopic yield point. To start with, In-doped specimens were stressed to above and below the yield point at 700°C at a strain rate of 10^{-4} s^{-1}.

Dislocation structures of undeformed and deformed specimens have been characterized by transmission electron microscopy. Specimens of GaAs and $Ga_{0.99}In_{0.01}As$ for TEM observations were made by cutting thin slices in a desired orientation, followed by mechanical polishing and ion-milling. These specimens were examined in a JEOL JEM 200CX transmission electron microscope at 200KeV using a double tilt goniometer stage. Characterization of dislocation structures has been performed by the standard g•b criterion. Electron microscopy results together with deformation data have been used to identify the mechanism of solid solution strengthening.

Crystals of compositions across the CdTe-MnTe phase diagram were

obtained from Professor Jack Furdyna of University of Notre Dame. Small crystal wafers of $Cd_{1-x}Mn_xTe$ ($0 < x < 0.6$) about 1 mm thick were cut parallel to the cleavage plane (110), polished first mechanically down to 0.25 micron diamond and then chemically in a solution of $K_2Cr_2O_7$-HNO_3-H_2O. The orientation was identified using cleaved edges and Vickers indentations were made with one of the diagonals parallel to [100] direction.

C. Technical Results:

Compression Tests

The results of uniaxial compression tests are summarized and compared with data from other investigations in Figures 1 and 2. Our results show that the critical resolved shear stress (CRSS) nearly doubled with In additions of $1\text{-}2\text{x}10^{20}$ atoms$\cdot$cm^{-3}. Also, the CRSS of both undoped and In-doped GaAs showed a weak temperature dependence, as expected from the solid solution strengthening model. The results also showed that the onset of dynamic recovery process in In-doped GaAs occurred at higher stress and strain levels suggesting that the climb process is more difficult in In-doped alloys compared to the undoped alloy. The strengthening observed seems sufficient to prevent macroscopic yield during the growth of large diameter GaAs crystals on the basis of current models of thermal stresses during crystal growth. These results and their interpretation are reported in detail in Appendix A.

The strain rate versus flow stress curves that were obtained also showed enhanced creep resistance by In-doping. Compression tests involving abrupt changes in strain rate were performed at 700°C, however, more tests at 900 and 1100°C are required to provide a good understanding of the strain rate dependence in this temperature range.

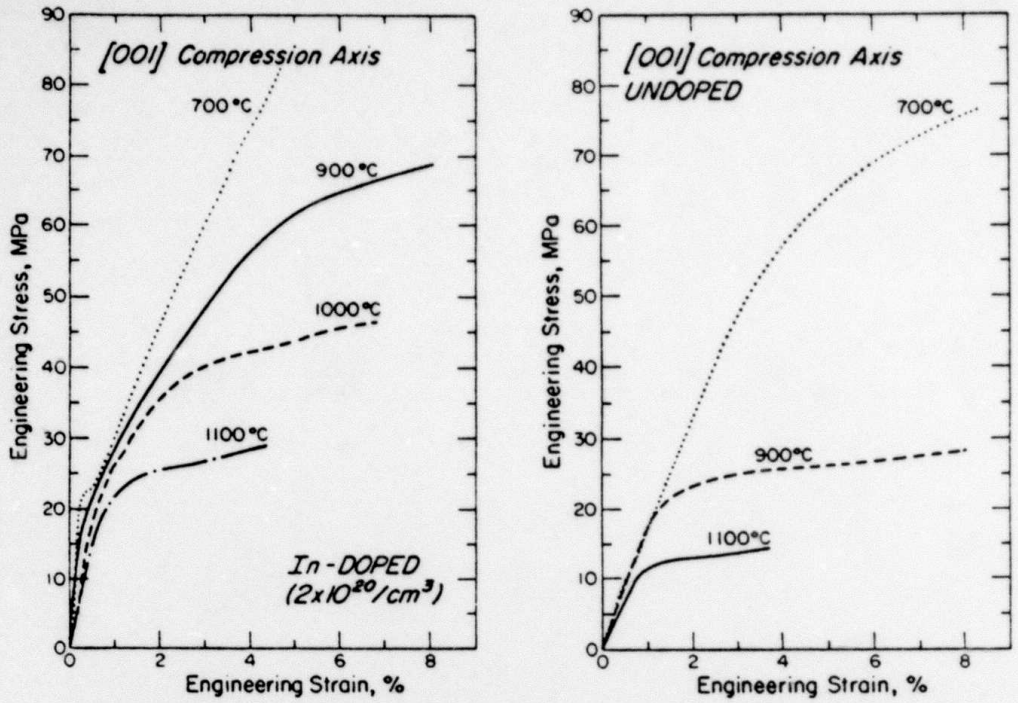

Figure 1. Engineering stress strain curves at different temperatures for (a) In-doped GaAs and (b) undoped GaAs specimens tested in the [001] orientation.

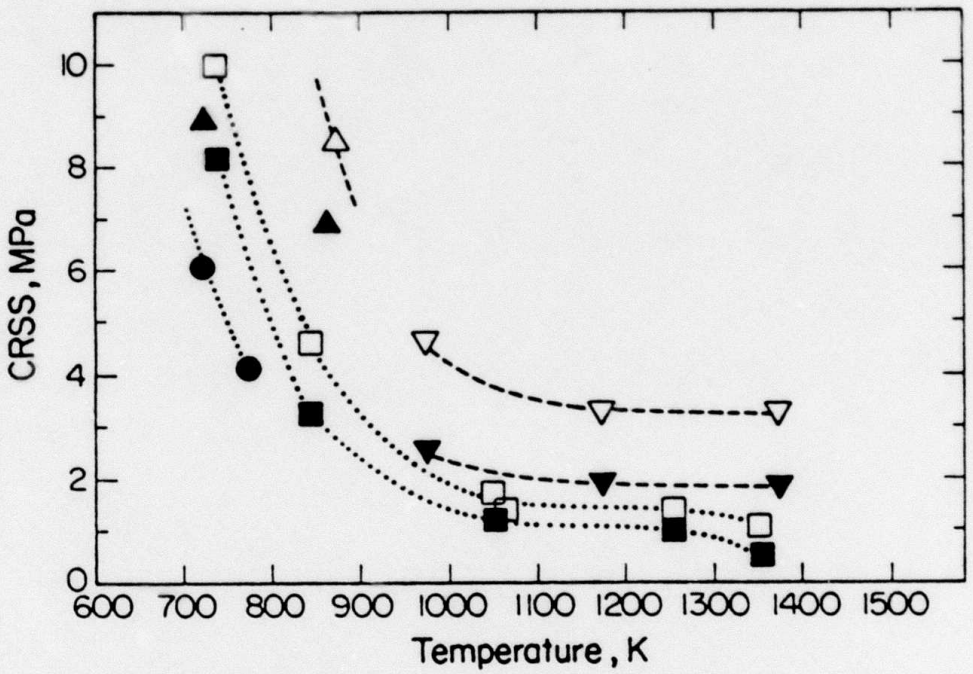

Figure 2. A comparison of the critical resolved shear stress values of undoped and In-doped GaAs as a function of temperature. Inverted open triangles, In-doped and inverted solid triangle, undoped (this study); open triangle, In-doped and solid triangles, undoped (S. McQuigan et al., 1986); solid squares, undoped (Tabache et al., 1986); solid circles (Swaminathan et al., 1975).

Transmission Electron Microscopy

Electron microscopy studies performed on undeformed specimens revealed very few dislocations. Most of the foil areas, particularly in the case of In doped GaAs were found to be dislocation free. If any dislocations were found, they were generally straight. In-doped and undoped GaAs specimens deformed at 500-700°C in the multiple slip orientation, [001], as well as in a single slip orientation, [123], revealed complex dislocation structures. The main dislocation structures were found to be dislocation dipoles (perfect as well as faulted), dislocation loops, arrays of small dislocation loops, dislocation tangles, dislocation networks and straight dislocations. Figure 3 shows a typical electron micrograph from a 500°C undoped GaAs specimen deformed to Stage II. Dislocation loops and faulted dipoles are clearly seen. Figure 4 shows an electron micrograph of In-doped GaAs deformed at 700°C to Stage II. Detailed analysis of dipoles and dislocation loops were done using dark-field weak beam pictures for $\pm g$ {220} type reflections. The break up of dipoles due to the mutual attraction of the positive and negative edge dislocations of its two elongated sides results in a row of loops. Dislocation loops were found to be of the vacancy type with Burgers vector a/3<111>. Further details are found in Appendix B.

Specimens in both single and multiple slip orientations deformed in the temperature range 900-1100°C have been taken to stage III to IV. Therefore, dislocation structures of these specimens were found to be fully recovered. Dislocation loops were rarely seen. The main dislocation structures found in these specimens were (i) parallel sets of dislocations having few interconnections (ii) hexagonal networks of dislocations and (iii) isolated dislocations. Figure 5, an electron micrograph of 900°C deformed In-doped GaAs, shows extended dislocations forming nodes. From

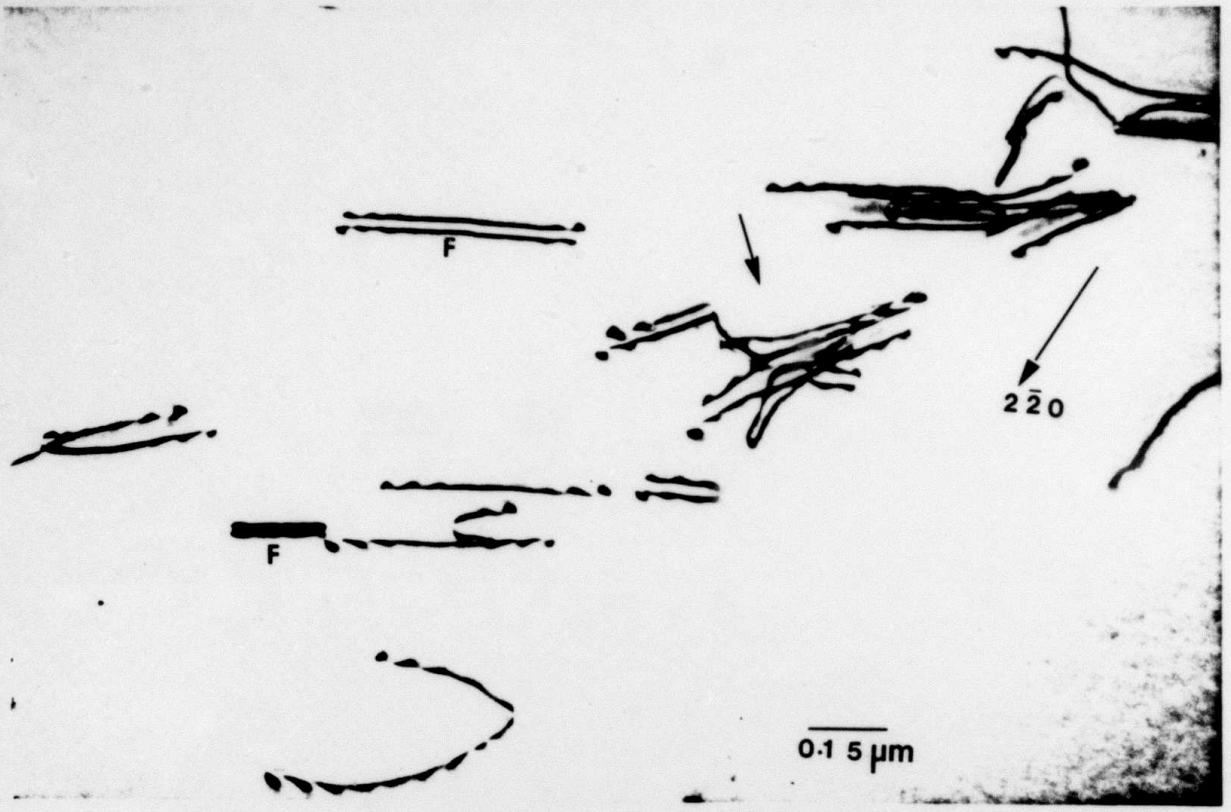

Figure 3. Electron micrograph of undoped GaAs deformed at 500°C to 3% strain. An array of dislocation loops (arrow) and faulted dipoles (F) are seen in the image. Zone axis = [001].

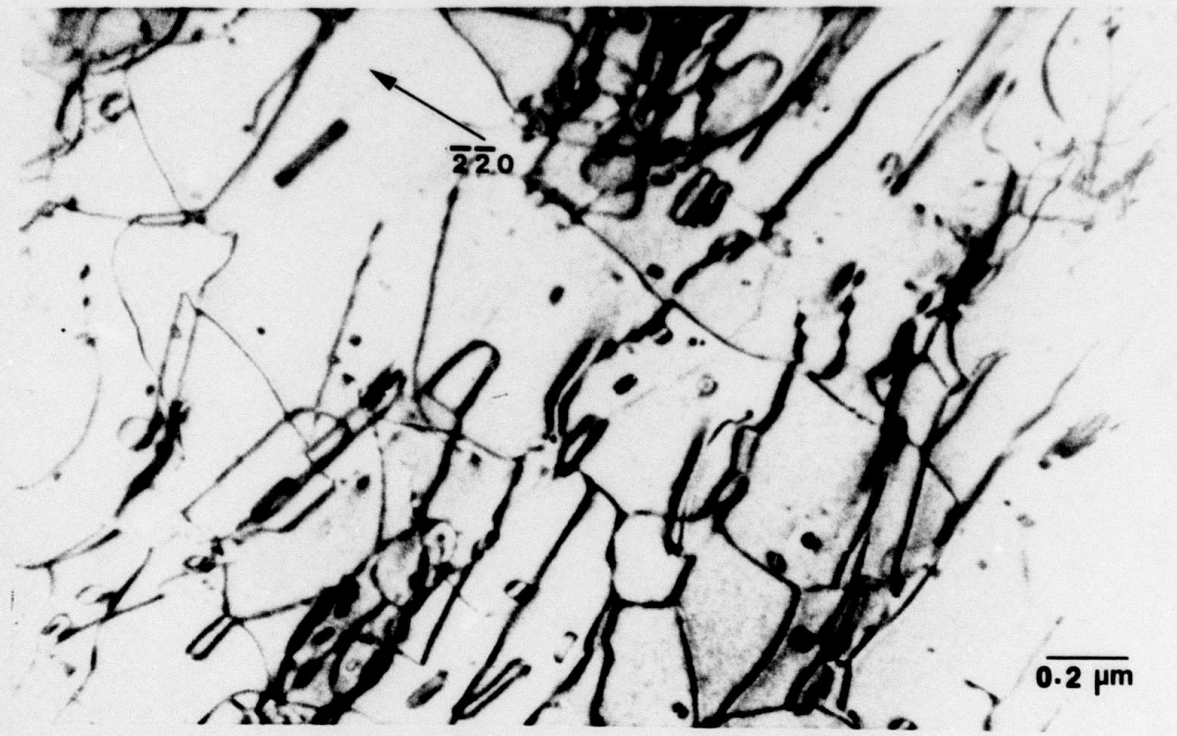

Figure 4. Electron micrograph of In-doped GaAs deformed at 700°C to 10% strain. The dislocation structures are typical of deformation Stages II-III. Zone axis = [$\bar{1}$11].

the weak beam pictures taken in different reflections, the majority of the dislocations in Figure 5 were found to be dissociated into two Shockley partials. Figure 6 shows parallel set of dislocations having few interconnections. This configuration of dislocations is an intermediate stage before recovery. In this configuration two out of plane 60° dislocations react to form a third dislocation in a screw orientation. The latter then reacts with a dislocation already present in the main slip plane and finally forms a hexagonal network in a screw orientation. Figure 7 shows such a hexagonal network. This type of dislocation structure indicates that climb process is dominant in the recovery of dislocated structures. Through numerous observations, recovery appears to be faster in the case of undoped GaAs compared to In-dope GaAs on the basis of dislocation structures present in the two cases. In addition, dislocation structures were found to be similar to those observed for Stage IV deformation of Si and Ge, a case where climb is known to be the dominant recovery mechanism.

The stacking fault energy has been estimated by measuring the separation of dissociated dislocations (from weak beam micrographs). The value of the stacking fault energy was found to be 45.3 $mJ \cdot m^{-2}$. No change in the value of stacking fault energy was found due to In doping, implying that there should be little influence on the cross-slip probability.

High Temperature Hardness of $Cd_{1-x}Mn_xTe$

Results on the hardness of five compositions of $Cd_{1-x}Mn_xTe$ are shown in Figure 8. Of the five compositions, $Cd_{0.91}Mn_{0.09}Te$ showed numerous twins during the optical microscopy examination and the measured hardness may not be representative of a single crystal. Interpretation of these results is forthcoming.

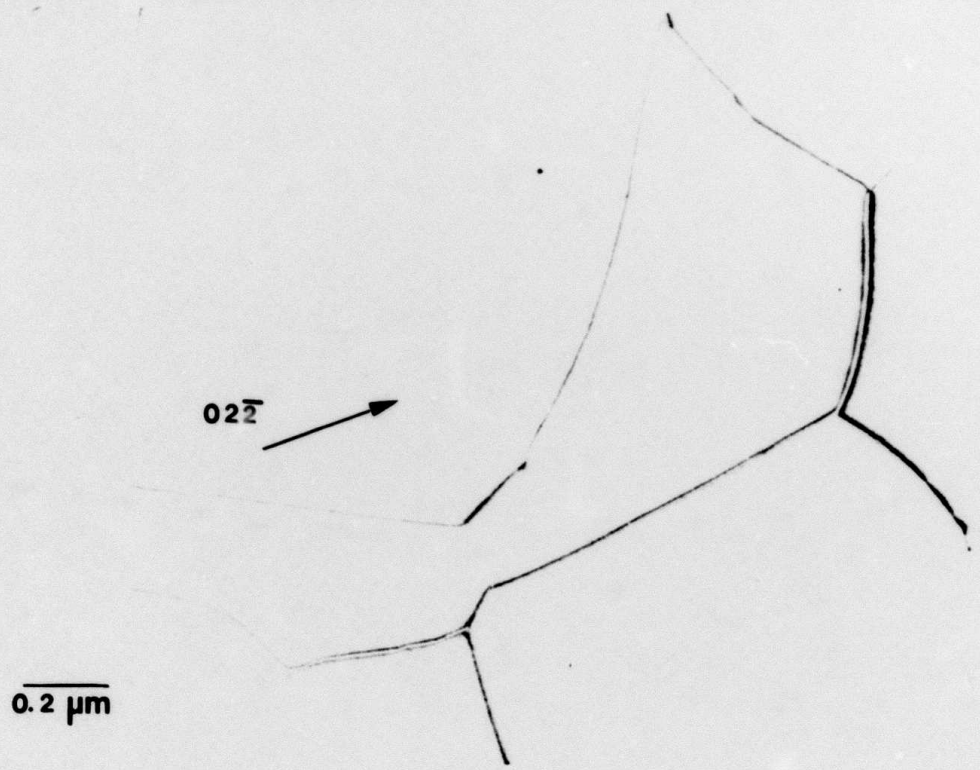

Figure 5. Electron micrograph of dislocation structures in In-doped GaAs deformed at 900°C for 5.1% strain. Zone axis = [$\bar{1}$11].

Figure 6. Electron micrograph of the intermediate stage dislocation configuration prior to recovery in In-doped GaAs deformed at 1000°C to 7.2% strain. Zone axis = [011].

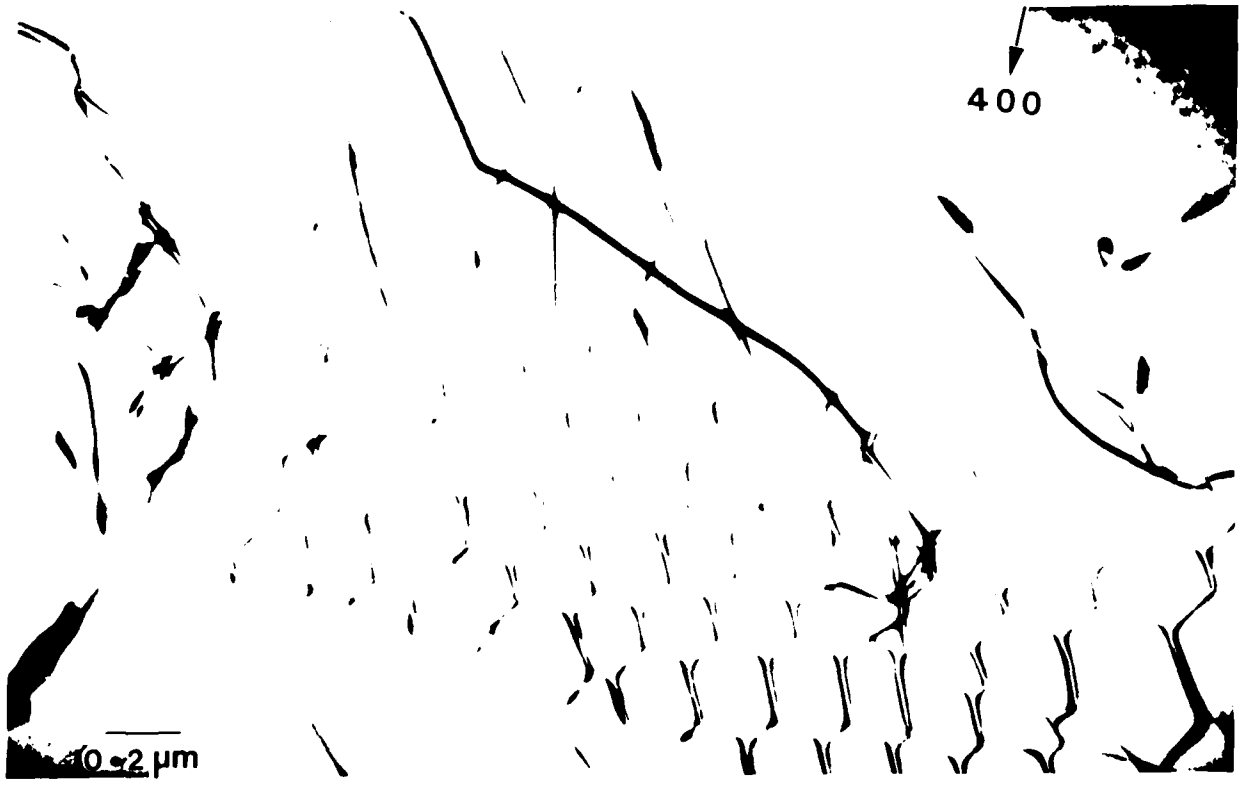

Figure 7. Electron micrograph showing well-recovered hexagonal networks of dislocations in In-doped GaAs deformed at 1000°C to 7.2% strain. Zone axis = [011].

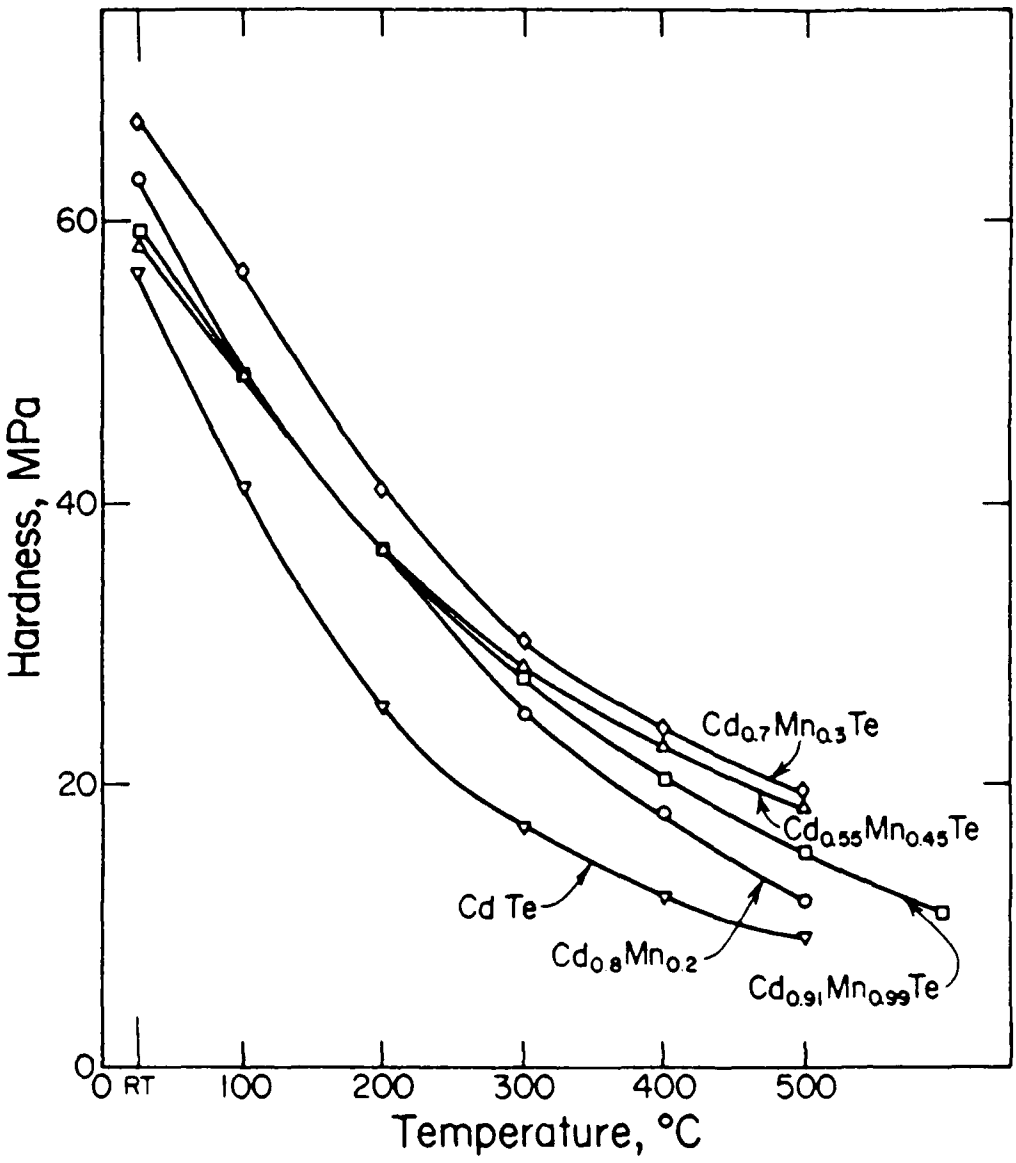

Figure 8. Vickers hardness versus temperature for $Cd_{1-x}Mn_xTe$ for $0<x<0.6$.

D. Implications for Future Research

Both the undoped and In-doped GaAs tested thus far contained large amounts of boron ($\approx 2 \times 10^{18}$ atoms$\cdot$cm^{-3}) which is also expected to be a potent isovalent solid solution strengthener. To isolate the effects of boron additions, tests of undoped GaAs containing two different amounts of boron are required. Undoped GaAs prepared by a modified Bridgman technique with varying boron content has now been obtained. Compression testing of these crystals in the [123] orientation at different strain rates and temperatures is in progress.

To better understand deformation during crystal growth, compression tests above 1100°C will be attempted. This should provide more significant data for extrapolation to the melting point of GaAs.

More transmission electron microscopy is planned for detailed analyses of dipoles and dislocation loops. Faulted dipoles will be studied with the combination of weak beam and high resolution transmission electron microscopy. From the high resolution imaging of faulted dipoles in In-doped and undoped GaAs a direct estimate of stacking fault energy can be accomplished. This value of stacking fault energy will be compared to the value obtained by measuring the separation of isolated dissociated dislocations. In addition, electron microscopy of high temperature deformed undoped GaAs with varying boron contents is planned in conjunction with the compression tests.

Further hardness and compression tests on II-VI compounds ($Cd_{1-x}Mn_xTe$) will continue following compression tests on undoped GaAs to examine solid solution strengthening in a variety of semiconductors.

E. Publications Enclosed with this Report

1. S. Guruswamy, R. S. Rai, K. T. Faber and J. P. Hirth, "Deformation Behavior of Undoped and In-doped GaAs in the Temperature Range 700°C, to appear in the Journal of Applied Physics, November 15, 1987. (Appendix A)

2. R. S. Rai, K. T. faber , S. Guruswamy and J. P. Hirth, "Transmission Electron Microscopy Studies in Deformed $Ga_{1-x}In_xAs$," pp. 320-31 in Proceedings of the 45th Annual Meeting of the Electron Microscopy Society of America (Ed. G. W. Baily) San Francisco Press, Inc., 1987.(Appendix B)

3. J. P. Hirth and A. G. Evans, Damage of coherent multilayer structures by injection of dislocations or cracks, J. Appl., Phys, **60** (7), 1 October 1986. (Appendix C)

APPENDIX A

To appear in J. Applied Physics,
November 15, 1987

Deformation Behavior of Undoped and In-doped GaAs in the Temperature Range 700°C to 1100°C

S. GURUSWAMY, R.S. RAI, K.T. FABER

Department of Ceramic Engineering

The Ohio State University, Columbus OH 43210

and

J.P. HIRTH

Department of Metallurgical Engineering

The Ohio State University, Columbus, OH 43210

ABSTRACT

Compressive deformation of undoped and In-doped GaAs single crystals has been carried out in [001] and [123] orientations in the temperature range 700 to 1100 °C. Indium additions, at levels of 1-2 x 10^{20} atoms.cm^{-3}, results in critical resolved shear stress (CRSS) values that are about twice as large as the undoped crystals in the temperature range of 700 to 1100°C. The CRSS was weakly dependent on temperature in the temperature range investigated as expected for a model of athermal solid solution hardening. The CRSS value of 3.3 MPa for the In-doped crystal is sufficient to eliminate profuse dislocation formation in a 75 mm diameter crystal on the basis of current theories for the magnitude of the thermal stress experienced during growth. The results also suggest that the process of dislocation climb is slowed appreciably by In-doping.

INTRODUCTION

Doping of GaAs with In, at a level of about 5 x 10^{19}-1x10^{20}/cm^3, in single crystals grown by the liquid encapsulated Czochralski process reduces the dislocation density from 10^4-10^5/cm^2 to $\leq 10^2$/cm^2.[1] The generation of dislocations during LEC growth in GaAs and other III-V compounds is believed to occur when the thermal stress imposed on the cyrstal during growth exceeds the critical resolved shear stress (CRSS).[2] Minimization of radial thermal gradients during growth and enhancement of the inherent strength of the crystal by the addition of isovalent as well as Group IV or VI elements can result in low dislocation density GaAs crystals.[3-5] Of the possible dopants, In has been found to be very effective and desirable because of its minimal influence on the electrical behavior of GaAs. Thermal stress calculations suggest that the maximum stress experienced is much larger than the extrapolated CRSS value of an undoped crystal.[6] The In doping, therefore, must result in a large increase in high temperature strength. It has been suggested that hardening akin to solid solution hardening occurs in $Ga_{1-x}In_xAs$ with an $InAs_4$ tetrahedral cluster being the solute unit that causes strengthening.[7] However, experimental data on high temperature deformation of GaAs and the influence of dopants is scarce and the role of In is still not well understood.

In a preliminary study, we first measured the temperature dependence of the hardness of undoped and In-doped GaAs, which was reported earlier.[8] In this subsequent study, we have evaluated the flow stress in the [001] orientation for which

multiple equivalent slip systems of (111) <110> type operate and in the [123] orientation suitable for the operation of only one slip system, $(\bar{1}11)[101]$. The results of the study made in the temperature range 700-1100°C are reported here, compared with other reported results,[6,9-13] and discussed in terms of models for the high temperature deformation of diamond cubic materials.[14,15]

EXPERIMENTAL PROCEDURE

The 75-mm diameter single crystals of semi-insulating GaAs and $Ga_{0.99}In_{0.01}As$ used in the present study were obtained from the Westinghouse R & D Center. The crystals were grown in [001] axial orientation. The undoped crystal had a dislocation density of 10^4-$10^5 cm^{-2}$. The indium doped crystal had an In concentration of about 1-2 x 10^{20}atoms.cm^{-3}. The boron concentration in both doped and undoped crystals was about 5 x 10^{17}atoms.cm^{-3}. The dimensions of specimens for compressive deformation in the [001] orientation were 5.3 mm x 5.3 mm x 10.6 mm in size with (110) and $(1\bar{1}0)$ lateral faces. The dimensions for deformation in the [123] orientation were 2.75 mm x 2.75 mm x 5.5 mm. The lateral faces were parallel to (111) or $(54\bar{1})$ planes. The specimen faces were mechanically polished to 0.3 μm alumina followed by chemical polishing in a 1% bromine-methanol solution. The specimen faces were parallel and orthogonal to within 0.5 degrees.

The compression testing was done on an INSTRON 1322 servohydraulic machine. A schematic diagram of the experimental

set up is shown in Figure 1. Tests were performed at temperatures of 700, 900, 1000 and 1100°C at a strain rate of $1 \times 10^{-4} s^{-1}$ in UHP argon. The furnace used in the study had a low heat capacity with a time of heat up to the test temperature of about 20 minutes. For tests at temperatures of 900°C and above the specimen was immersed in B_2O_3 liquid. The compression rams used were made of high purity alumina, and a special fixture made of alumina was used for the alignment and positioning of the specimen. The elongation was measured on the alumina rams by means of an extensometer and was corrected for the fixture compliance, measured at temperature, in converting the data to strain.

Stress relaxation tests were performed following the [001] specimen compression tests. At the end of compressive deformation, the decrease in stress at constant specimen length was measured as a function of time and was converted to plastic strain as a function of time. The total amount of strain during stress relaxation is very small and the total time of testing is only a few minutes.

RESULTS

(A) [001] Orientation

Figures 2a and 2b show the results of compression tests in [001] orientation for undoped and In-doped GaAs. No easy glide, stage I deformation is observed for these crystals, oriented for multiple slip. Also, only at 700°C for the In-doped case is there an indication of the yield point phenomena characteristic of a similar material[6] tested at 350 to 590°C. The tendency for less

pronounced yield point with increasing temperature is consistent with results in other studies,[6,10] and the absence of well-defined yield points at high temperatures agrees with the work of Djemel et al.[11] We note that the slope below the yield point at 700°C for the In-doped case is less than the reported elastic modulus so that microyield and plastic flow are already occurring. This characteristic has been observed in other measurements,[6,10,11] including those at lower temperatures. Indeed, in-situ X-ray topographic measurements made during tensile testing of In-doped and undoped GaAs at 450-700°C demonstrate directly that dislocation formation and propagation occur at stresses well below the upper yield point.[16,17] Such phenomena are well known for metals where microyield also occurs well below the macroscopic yield point[18] with sufficient mobility and multiplication rates for dislocations as can occur at high temperatures. The microyield regime A[19] merges smoothly into stage II deformation behavior.

The stress-strain curves, with the exception of the In-doped 700°C case, are characterized by a stage II linear work hardening regime of flow, followed by stage III characterized by a decrease in work hardening rate, and the beginning of the stage IV linear hardening regime characteristic of diamond cubic materials.[14,15,20]

The results indicate hardening effects by indium in all stages of deformation. The stage A slopes increase with decreasing temperature and are larger at all temperatures for the In-doped crystals. The onset of stage III occurs at larger stresses in the In-doped case, and the slope in stage IV is

greater for the In-doped case. A yield point, indicative of insufficient dislocation mobility/multiplication, occurs for the In-doped crystals at 700°C but not for the undoped crystals. Also, for the 700°C case, the microyield flow region A, below the yield point, has a larger slope (larger work hardening) than the post-yield, stage II, linear work hardening regime.

Values for the 0.2% offset yield strength from the present work and that of others are presented in Table I and plotted in Figure 3. The data are all converted to critical resolved shear stresses for later comparison with single slip crystals. The agreement shown in Figure 3 is seen to be quite good.

(B) [123] Orientation

The specimens tested in [123] orientation showed sharp yield points. Flow stress-strain curves for undoped and In-doped specimens at 700°C are shown in Figure 4. The single slip orientation cyrstals showed extensive stage I deformation with a small yield drop at 700°C (Figure 4), but not at 900 or 1100°C. The pre-yield slopes in the microyield region A varied just as in the [001] case, with smaller slopes for the undoped case at each temperature and with a decrease in slope with increasing temperature.

In comparison, the suppression of yield point phenomena at temperatures above 700°C for [001] crystals (present work, ref. 11) indicates a strong impediment to dislocation intersection in these crystals. This impediment, favored by the relatively low stacking fault energy of ~45 mJ/m^2 in these materials,[21] suppresses easy glide and contributes to the large stage II slope

for the [001] crystal. Neverthless, the dislocation mobility in stage II is sufficient to prevent macroscopic yield point behavior.

The values for the upper yield point as a function of temperature, together with results from other work, are listed in Table I and plotted in Figure 5. Lower temperature data for [100] specimens from the work of Hobgood et al.[6] and Swaminathan and Copley[9] are included because their specimens also exhibited sharp yield points with little yield drop. This [001] yield point behavior below 700°C is associated with the reduction in dislocation multiplication/mobility by the presence of the peierls barrier and the attendant mechanism of double-kink dislocation motion.

The present results align well with the other work on the same material.[6,9,10] All results are in agreement with regard to the general shape of the curves of flow stress versus temperature. However the present results are consistently higher in stress, by about a factor of two, than the other extensive work on single slip crystals.[10] A possible cause for this difference, as discussed previously[8] is the presence of $\sim 5 \times 10^{17} cm^{-3}$ of boron in the present samples, a solute that would also be expected to produce strong solution hardening.

DISCUSSION

(A) Compression Tests

The overall form of the stress-strain curves with stages II to IV for [001] crystals, and stage I, as well, for [123] crystals, is consistent with the behavior at elevated temperatures of the

much more extensively studied Si and Ge crystals.[14,15,20] The analogy suggests that glide processes are important in determining the flow stress in stages I and II while recovery processes are important, in addition, in stages III and IV. The relative temperature independence of the critical resolved shear stress above 700°C (Figures 3 and 5), implies plateau-type behavior[22] characteristic of athermal solid solution hardening. Hence, the hardening indicated at yield and in stage I is consistent with the suggestion[7] that In should provide strong solid solution hardening in $Ga_{1-x}In_xAs$.

Below ~700°C, the sharp rise in flow stress with decreasing temperature is related to a change in the mechanism of glide to one controlled by double-kink nucleation and propagation, again analogous to Si and Ge. The hardening effect in this regime could also be related to the elastic field of an $InAs_4$ unit,[7] in this case effective through an impediment to the propagation of kinks along a dislocation line. Because of the apparent change of mechanism below about 700°C, results obtained below this temperature, e.g. on dislocation velocity,[23,24] may not be applicable to behavior above 700°C.

The larger stress for the onset of stage III and the larger slope in stage IV for In-doped crystals imply a decrease in recovery rate for the In-doped crystals. This could be caused, in principle, by suppression of cross-slip or by retardation of climb. Several factors indicate that the latter climb effect is predominant. First, transmission electron microscopy studies[21] indicate that In-doping, at the level studied here, does not

affect the stacking fault energy, implying that there should be little influence on the cross-slip probability. Second, our transmission electron microscopy studies[25] of [001] specimens strained into stage IV show well developed dislocation networks similar to structures observed for stage IV deformation of Si,[20] a case where climb is known to be the dominant recovery mechanism. Third, stress relaxation measurements in the present work[26] show consistently lower relaxation rates for the In-doped case at a given stress over the entire range of relaxation, implying a lower climb rate.

(B) Comparison with Hardness Results

Resolved shear stress values calculated earlier by us from values of the hardness H [8] are much higher than the measured flow stress values. Comparative data using the earlier estimate of H/6 together with 4% offset flow stresses are listed in Table I. The reason for the discrepancy is our earlier use of an empirical correlation of hardness and yield strength for engineering materials with characteristically low work hardening rates. If, instead, the strain hardening rates are taken into account using the empirical relationship developed by Cohoon et al.,[27] $(H/\sigma_{7.4}) = 3 \times 10^{n}$ where n is the strain hardening exponent, and $\sigma_{7.4}$ is the flow stress at 7.4% strain, the values of flow stress calculated from hardness values approach the flow stress at 4% strain, but still appreciably exceed the 0.2% offset yield stress. The trends in hardness with temperature and the hardening increment provided by indium as revealed in the earlier work, however, do give an indication of the strengthening effect of In consistent with the present work.

(C) Crystal Growth

Recent calculations by Jordan et al.[28] indicate that dislocations can be completely removed in 75 mm diameter GaAs crystals grown under low thermal gradient conditions if the CRSS for plastic flow initiation is a factor of four larger than a GaAs base level value of 0.6 MPa, determined by extrapolation to the melting point. The basis for the extrapolation is the data for the yield point of undoped GaAs (ref. 9, Figure 3). The present results, Figure 3 and 5, suggest a value of 3.3 MPa for the yield point extrapolated to the melting point for the present case of In at a level of 1-2 x $10^{20}cm^{-3}$. Hence, such a doping level of indium should prevent the profuse dislocation generation characteristic of stage I deformation according to the theory of Jordon et al.[28]

However, the present work and that of others[6,10,11] show that microyield occurs well below the yield point in compression tests above 700°C and particularly at 1100°C. These results, together with the in situ, X-ray topographic studies in tension[16,17] at temperatures less than 700 °C , indicate that dislocations, once formed, are highly mobile at high temperatures. This suggests that, if GaAs crystals are grown in a dislocation-free condition, a major impediment to the presence of dislocations must be the nucleation process. In all of the compression tests [present work, refs. 6, 9, 10, 11] the crystal end in contact with the loading platens is an easy site for dislocation nucleation because of stress intensification at contact asperities and because of the weak singularity in the stress

field at the edge of the contact surface of the specimen. Hence, such data, while indicative of the yield point, may not correspond in microyield behavior to the crystal growth case where nucleation of dislocations would be more difficult. There is some indication of such a possibility in the low temperature tensile test observations of Tohno et al.,[16,17] a case where such end effects are absent and where dislocation nucleation does not occur at stresses of at least twenty percent of the yield stress.

SUMMARY

(A) Addition of In at levels of 1-2 x 10^{20} atoms/cm^3 results in CRSS values for flow that are about twice as large as the undoped crystals throughout the stress-strain curve and in the temperature range of 700 to 1100°C.

(B) The CRSS for a yield point or for the 0.2% offset yield strength was weakly dependent on temperature in the temperature range investigated as expected for a model of athermal solid solution hardening.

(C) The strength of In-doped crystal is sufficient to eliminate profuse dislocation formation in a 75 mm diameter crystal on the basis of current theories for the magnitude of the thermal stress during growth.

(D) The onset of stage III occurs at much higher stress levels in the In-doped alloy. Together with observations of dislocation structures, this suggests that the process of dislocation climb is slowed appreciably by In-doping.

ACKNOWLEDGEMENTS

The authors are grateful for the support of this work by the Defence Advanced Research Projects Agency (DOD), Order No. 5526, monitored by AFOSR under Contract No. F49620-85-C-0129, and for the provision of materials for this research by Dr. Shaun McGuigan of the Materials Growth and Device Technology Group, Westinghouse R & D Center under their contract with DARPA, No. N00014-84-C-0632.

REFERENCES

[1]S. McGuigan, R. N. Thomas, D. L. Barret, H. M. Hobgood and B. W. Swanson, Appl. Phys. Lett. **48**, 1377 (1986).

[2]A. S. Jordon, A. R. Von Neida, and R. Caruso, J. Crys. Growth 70, 555 (1984).

[3]Y. Seki, H. Watanabe and J. Matsui, J. Appl. Phys., **49**, 822 (1978).

[4]N. P. Sazhin, M. G. Milvidskii, V. B. Osvenskii and O. G. Stoljarov, Soviet Phys.-Solid State, **8**, 1223 (1966).

[5]G. T. Brown, B. Cockayne and W. R. MacEwan, J. Crystal Growth, **51**, 369 (1981).

[6]H. M. Hobgood, S. McGuigan, J. A. Spirotznagel and R. N. Thomas, Appl. Phys. Lett, **48**, 1654 (1986).

[7]H. Ehrenreich and J. P. Hirth, Appl. Phys. Lett., **46**, 668 (1985).

[8]S. Guruswamy, J. P. Hirth and K. T. Faber, J. Appl. Phys., **60**, 4136, (1986).

[9]V. Swaminathan and S. M. Copely, J. Amer. Ceram. Soc., **58**, 482 (1975).

[10]M. G. Tabache, E. D. Bourett and A. G. Elliot, Appl. Phys. Lett., **49**, 289 (1986).

[11]A. Djemel and J. Castaing, Europhys. Letts., **2**, 611 (1986).

[12]D. Laister and G. M. Jenkins, J. Mater. Sci., **8**, 1218 (1973).

[13]I. Yonenaga, U. Onose and K. Sumino, J. Mater. Res. **2**(1987) 252

[14]H. Siethoff and W. Schroeter, Z. Metall., **75** 475 (1984).

[15]W. Schroeter and H. Siethoff, Z. Metall., **75**, 482 (1984).

[16]S. Tohno, S. Shinoyama, A. Katsui and H. Takaoka, Appl. Phys. Lett, **49** 1206 (1986).

[17]S. Tohno, S. Shinoyama, A. Katsui and H. Takaoka, J. Crystal Growth, 73, 190 (1985).

[18]F. R. N. Nabarro, Z. S. Basinski and D. B. Holt, Adv. in Phys., 13, 193 (1964).

[19]In conventional deformation of metals at room temperature, only stages I through V of plastic flow are identified. It is recognized for metals that microyield occurs well below the yield point,[18] but the amount of microyield strain is so small that deviations of the slope of the stress-strain curve from the linear elastic value are usually not detected. In the present higher temperature case, and, one would expect, for metals at high temperatures as well, the slope does deviate appreciably from the elastic value, so we have identified the flow region as stage A.

[20]H. G. Brion and P. Haasen, Phil. Mag. A., 51, 879 (1985).

[21]M. Jimenex-Melendo, A. Djemel, J. P. Riviere and J. Castaing, in Defects in Semiconductors, ed. by H. J. Von Bardeleben (Trans. Tech. Publications, 1986), Materials Science Forum, Vol. 10-12 (1986), pp. 791-796.

[22]P. Haasen, in Dislocations in Solids, ed. by F. R. N. Nabarro (North Holland, Amsterdam, 1982), Vol. 4., p. 147.

[23]I. Yonenaga, K. Sumino and K. Yamada, Appl. Phys. Lett., 48, 326 (1986).

[24]M. Matsui and T. Yokoyama, Int. Symposium on GaAs and Related Compounds, Japan Int. Prop. Conference Series No. 79, 1985, Chap. 1, p. 13.

[25]R.S. Rai, K.T. Faber, S. Guruswamy and J.P. Hirth, Proc. 45 th Annual meeting of Electron Microscopy Society of America, ed. by G.W. Bailey (San Francisco Press, Inc., 1987) pp. 320-321.

[26]S. Guruswamy, R.S. Rai, K.T. Faber and J.P. Hirth, unpublished.

[27]J. P. Cohoon, W. H. Broughton and A. R. Kutzak, Met. Trans., 2, 1979 (1971).

[28]A. S. Jordon, A. R. Von Neida and R. Caruso, J. Crystal Growth, 76, 243 (1986).

FIGURE CAPTIONS

Figure 1. Schematic of the compression testing jig.

Figure 2. Engineering stress strain curves at different temperatures for a) In-doped GaAs and b) undoped GaAs specimens tested in the [001] orientation.

Figure 3. Comparison of critical resolved shear stress values of undoped and In-doped GaAs from present and other work in the [001] orientation as a function of temperature. Open squares, In-doped (this study); solid squares, undoped (this study); open triangle, In-doped (Ref.6); solid triangle, undoped (Ref. 6); open circles, In-doped (Ref. 11); solid circles, undoped (Ref. 11).

Figure 4. Engineering stress strain curves for undoped and In-doped GaAs in the [123] orientation.

Figure 5. Comparison of critical resolved shear stress values of undoped and In-doped GaAs from present and other work as a function of temperature. Inverted open triangle, In-doped (this study); inverted solid triangle, undoped (this study); open triangle, In-doped (Ref. 6); solid triangles, undoped (Ref. 6); open squares, In-doped (Ref. 10); solid squares, undoped (Ref. 10); solid circles, undoped (Ref. 9).

Table I. Resolved shear stress values for undoped and In-doped GaAs.

σ_Y is upper yield point, $\sigma_{0.002}$ and $\sigma_{0.04}$ are offset yield strengths at strains of 0.002 and 0.04, respectively, and H/6 is an estimate from data for hardness H. Numbers in parentheses are references to other work.

		[123] orientation	[001] orientation			
Material	T(K)	σ_Y(M Pa)	σ_Y (MPa)	$\sigma_{0.002}$ (MPa)	$\sigma_{0.04}$ (MPa)	H/6 (MPa)
	973	4.64	-	9.3	27.8	66.7
In-doped GaAs	1173	3.33	-	8.8	23.1	39.9
	1273	-	-	8.5	17.2	-
	1373	3.27	-	7.8	11.6	-
	973	2.55	-	2.8	21.8	51.7
Undoped GaAs	1173	1.91	-	2.45	10.0	28.6
	1373	1.83	-	2.45	6.0	-
	1253	1.4 (10)				
	1353	1.05 (10)				
In-doped GaAs (LEC)						
	873		8.5 (6)			
			5.5 (6)			
	800			9.6 (11)		
	900			7.6 (11)		
	1053			7.2 (11)		
	1053	1.22 (10)				
	1253	1.0 (10)				
	1353	0.53 (10)				
Undoped GaAs (LEC)	873		6.9 (6)			
	800			2.2 (11)		
	900			2.1 (11)		
	1053			2.2 (11)		
	773	3.9 (13)				
Undoped GaAs (non LEC)	823		2.4 (9)			

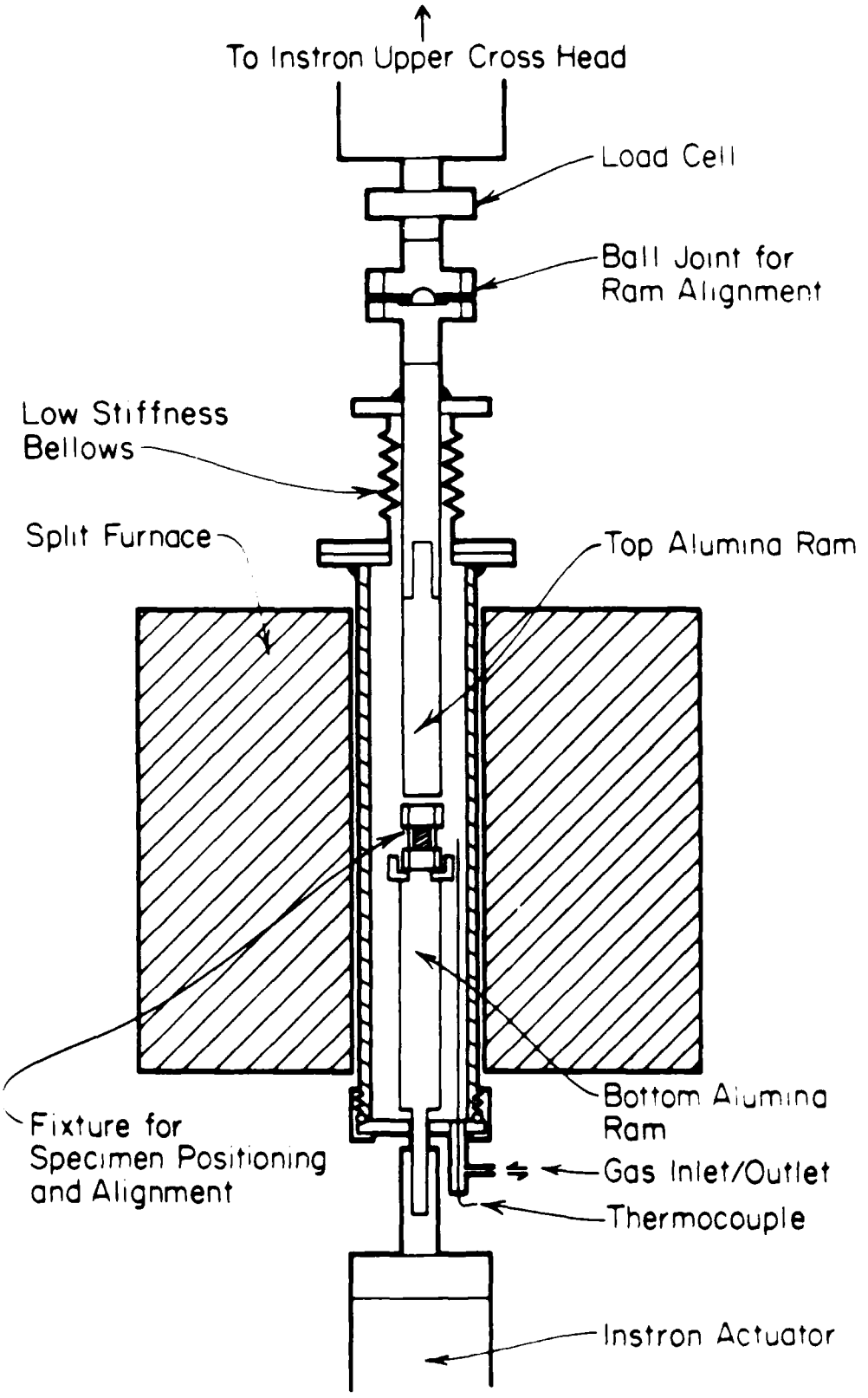

Figure 1. Schematic of the compression testing jig.

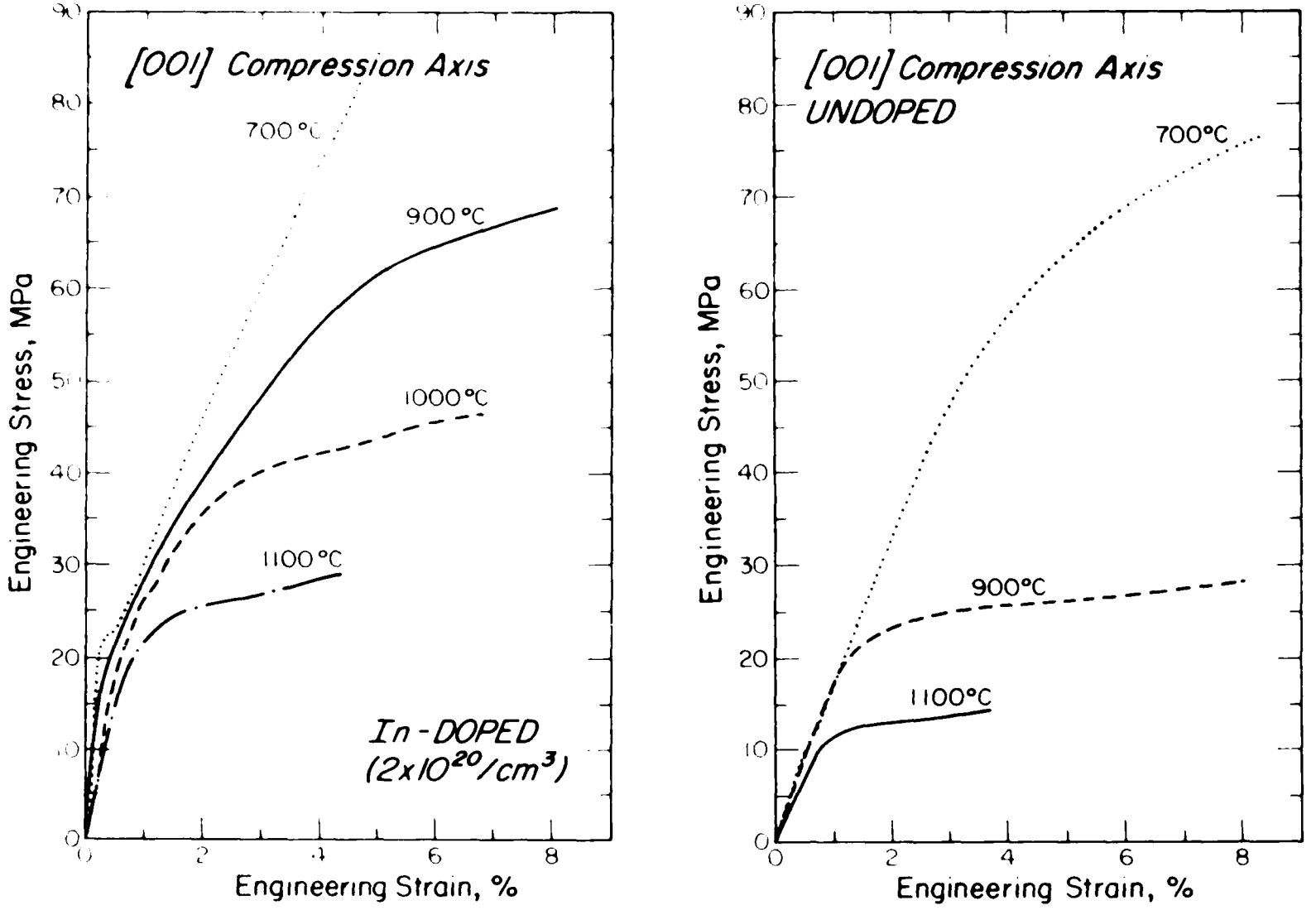

Figure 2. Engineering stress strain curves at different temperatures for a) In-doped GaAs and b) undoped GaAs specimens tested in the [001] orientation.

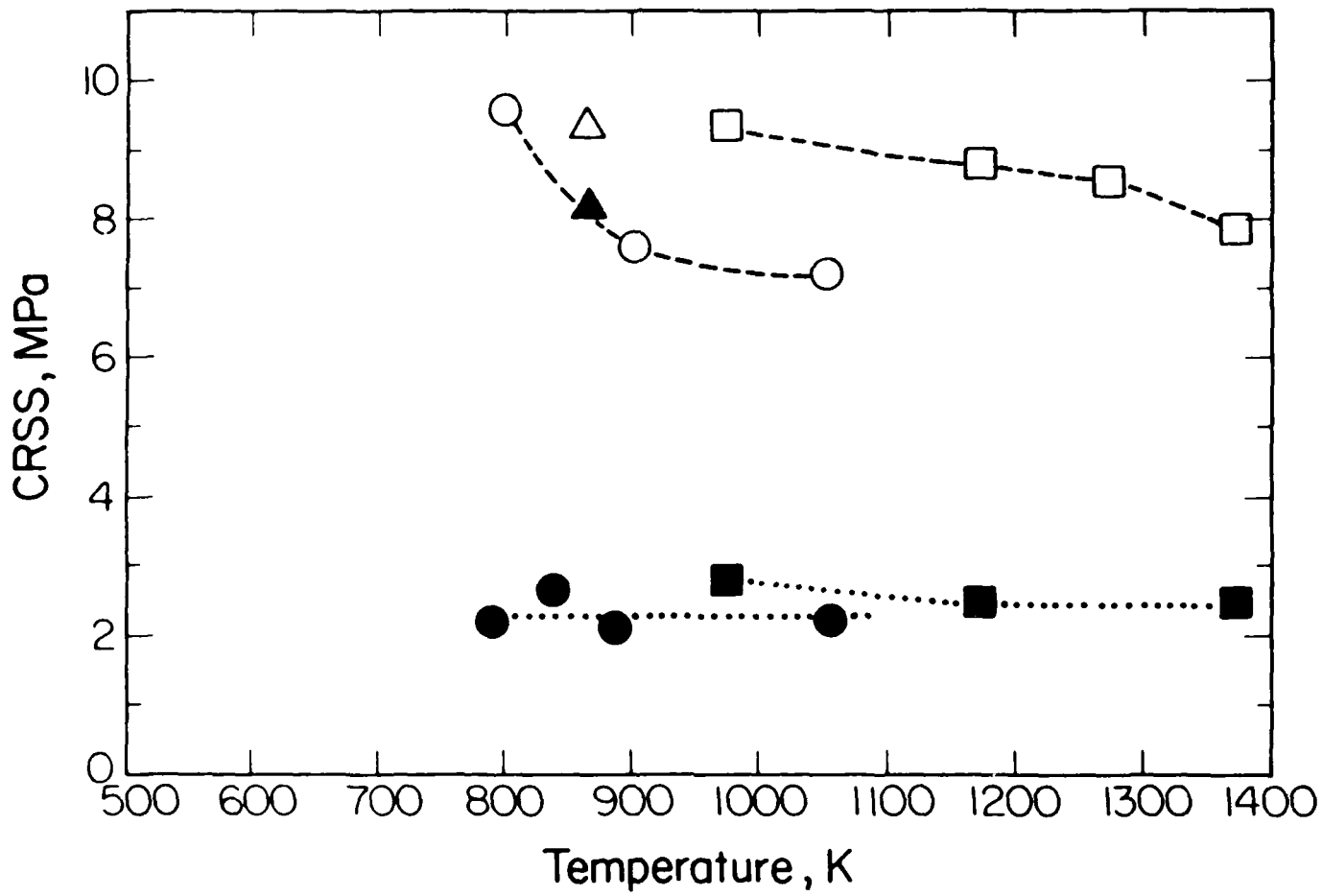

Figure 3. Comparison of critical resolved shear stress values of undoped and In-doped GaAs from present and other work in the [001] orientation as a function of temperature. Open squares, In-doped (this study); solid squares, undoped (this study); open triangle, In-doped (Ref.6); solid triangle, undoped (Ref. 6); open circles, In-doped (Ref. 11); solid circles, undoped (Ref. 11).

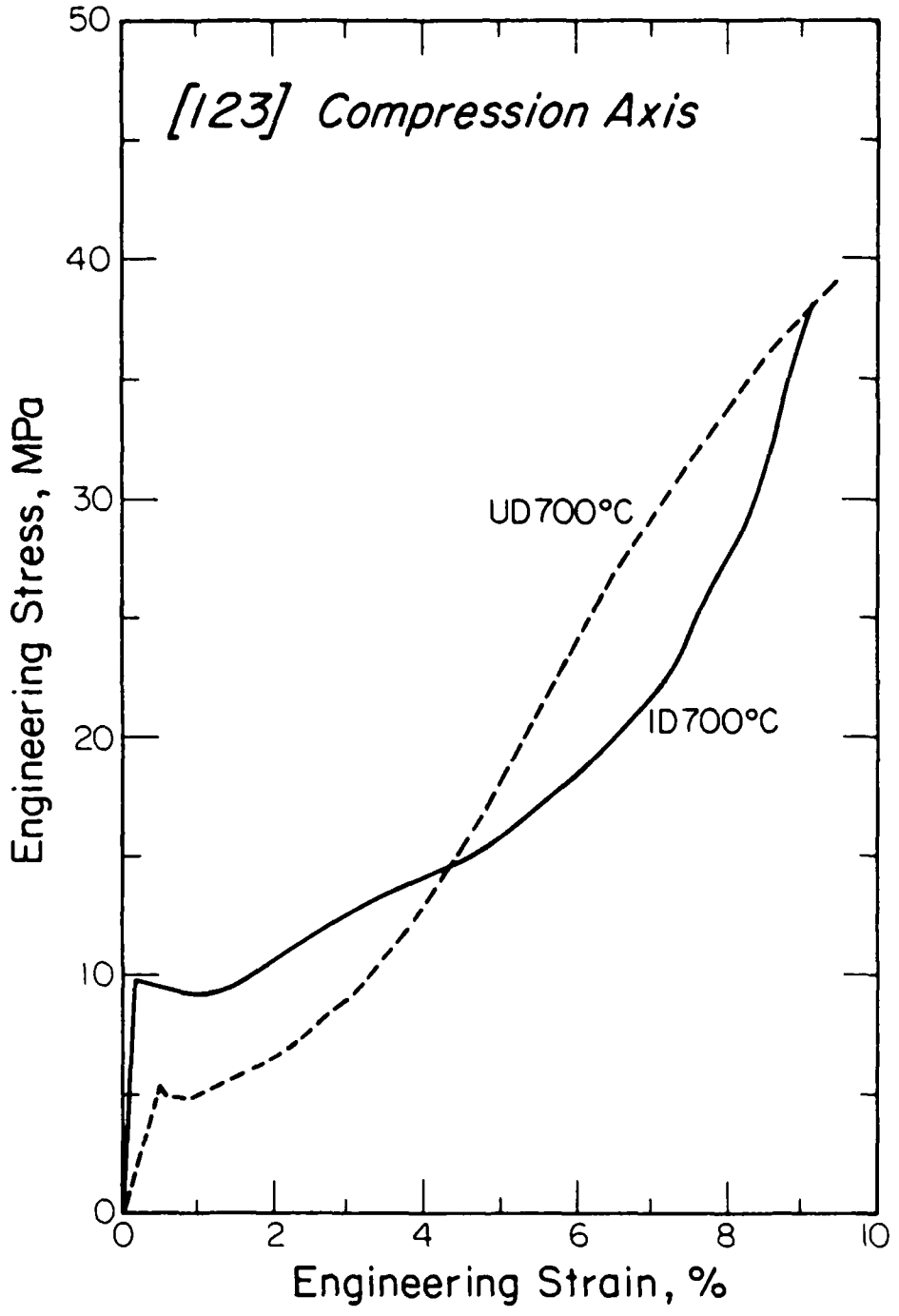

Figure 4. Engineering stress strain curves for undoped and In-doped GaAs in the [123] orientation.

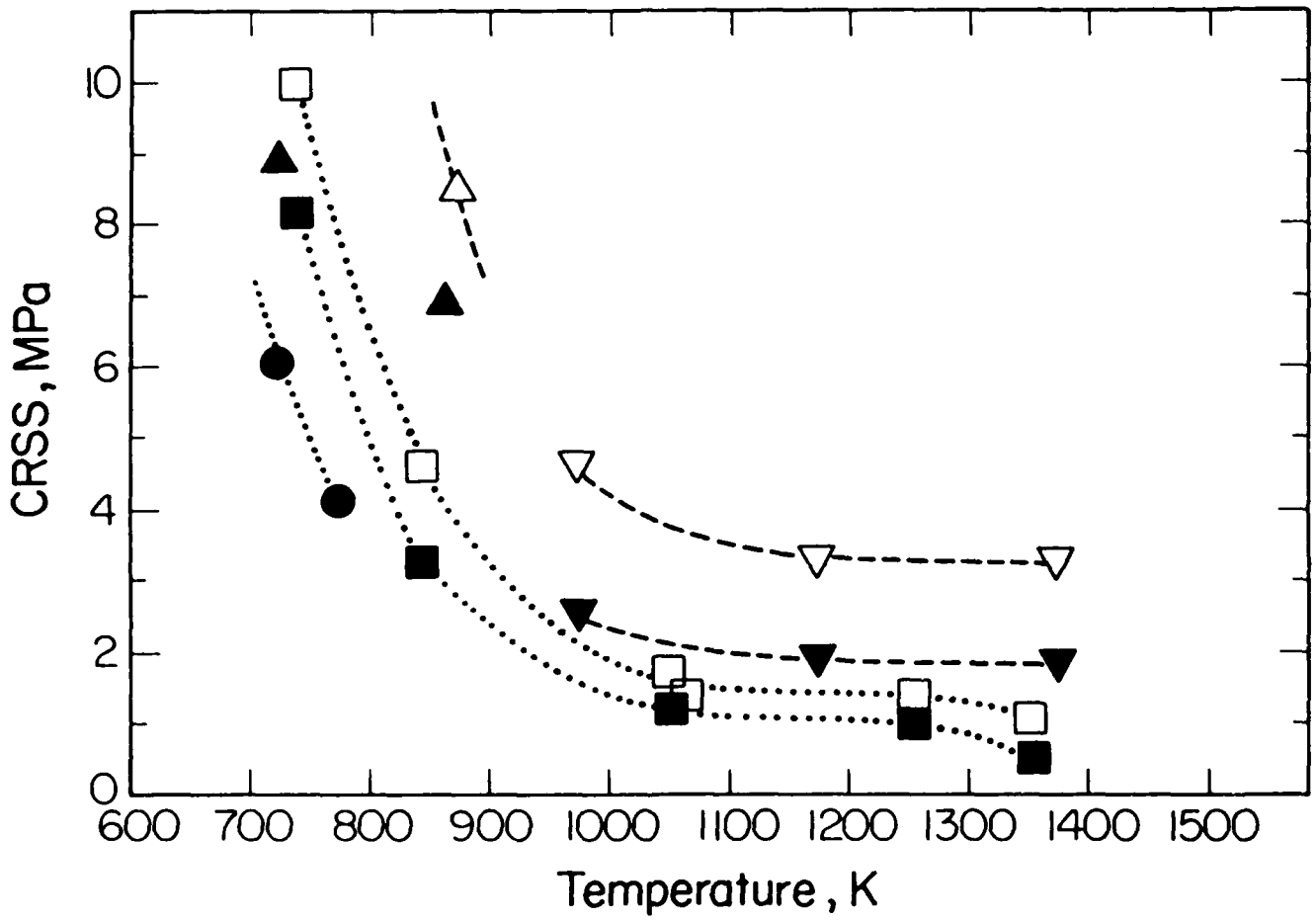

Figure 5. Comparison of critical resolved shear stress values of undoped and In-doped GaAs from present and other work as a function of temperature. Inverted open triangle, In-doped (this study); inverted solid triangle, undoped (this study); open triangle, In-doped (Ref. 6); solid triangles, undoped (Ref. 6); open squares, In-doped (Ref. 10); solid squares, undoped (Ref. 10); solid circles, undoped (Ref. 9).

APPENDIX B

G. W. Bailey, Ed., *Proceedings of the 45th Annual Meeting of the Electron Microscopy Society of America*

TRANSMISSION ELECTRON MICROSCOPY STUDIES IN DEFORMED $Ga_xIn_{1-x}As$

R. S. Rai,* K. T. Faber,* S. Guruswamy,* and J. P. Hirth**

* Department of Ceramic Engineering, and **Department of Metallurgical Engineering, The Ohio State University, Columbus, Ohio 43210

The control of dislocation density during the growth of GaAs and related compounds is highly desirable for obtaining improved performance and reliability of opto-electronic devices. Doping of single crystal GaAs grown by the LEC process with Indium has been known to reduce the dislocation density significantly.[1] Substitutional solid-solution strengthening of GaAs as an InAs unit has been suggested to be responsible for reduction of dislocation density.[2,3] To understand the mechanism involved in dislocation density reduction, deformation tests have been performed on [001] oriented $Ga_xIn_{1-x}As$ single crystals in the temperature range 700-1100°C and this paper reports some results of the TEM characterization of dislocations in these deformed single crystals.

Specimens of GaAs and $Ga_{0.99}In_{0.01}As$ for TEM observations were made by cutting thin slices in a desired orientation, followed by mechanical polishing and ion-milling. These specimens were examined in a JEOL JEM 200CX transmission electron microscope at 200KeV equipped with a double-tilt goniometer stage.

In GaAs, owing to its polarity, two types of dislocations with opposite Burgers vectors, termed α and β, can be distinguished. Both dislocation types were found in the present study. Edge character dominated in the higher temperature deformed specimens in contrast with the low temperature undoped deformed specimens where screw dislocations dominate.[4] In the 700° deformed specimens, In-doped and undoped both show the presence of small dislocation loops, complex dislocations networks and some isolated dislocations. Only in case of the In-doped specimens, straight dislocations lying along <110> directions are seen in some regions. An example of the dislocation structure in the 700°C undoped specimen is shown in Fig.1. In a few places, dislocations are dissociated into two Shockley partials. The dislocations have been characterized using the standard g.b criterion. For partial dislocations, the analysis was carried out with the help of weak beam pictures taken in <220> type reflections.

Specimens deformed at 1000 and 1100°C show quite relaxed dislocation structures compared to the 700°C case. Hexagonal networks of dislocations, parallel sets of dislocations intersected by dislocations of different slip systems, as well as isolated dislocations were found. Fig.2 shows hexagonal networks of dislocations in the 1000°C deformed In-doped specimen. Dislocations of one set are clearly dissociated into two Shockley partials. One interesting example is shown in Fig.3 where dislocation lines lie nearly along <110> and <112> directions. Most of the dislocations in these configurations were found to be dissociated. The dissociation scheme $a/2[101] \longrightarrow a/6[211] + a/6[1\bar{1}2]$ for dislocations A (marked in Fig.3) is the expected one that forms an intrinsic stacking fault.

From this study, dislocation structures in these $Ga_xIn_{1-x}As$ alloys consist of dislocation loops, networks of dislocations and isolated dislocation dipoles. A detailed TEM study of deformed specimens is still in progress and will be reported elsewhere.[5]

References

1. R.N. Thomas (private communication).
2. H. Ehrenreich and J.P. Hirth, Appl. Phy. Lett. (1985) 46, 668.

3. S. Guruswamy, J.P. Hirth and K.T. Faber, J. Appl. Phys. (1986) 60, 4136.
4. K.H. Kuesters, B.C. DeCooman and C.B. Carter, Phil. Mag. (1986) A53,141.
5. This work was supported by DARPA Order No. 5526, monitored by AFOSR under Contract No. F49620-85-C-0129 and the materials were supplied by Westinghouse R&D Center under their contract with DARPA, No. DARPA-Westinghouse-N-0014-84-C-0632.

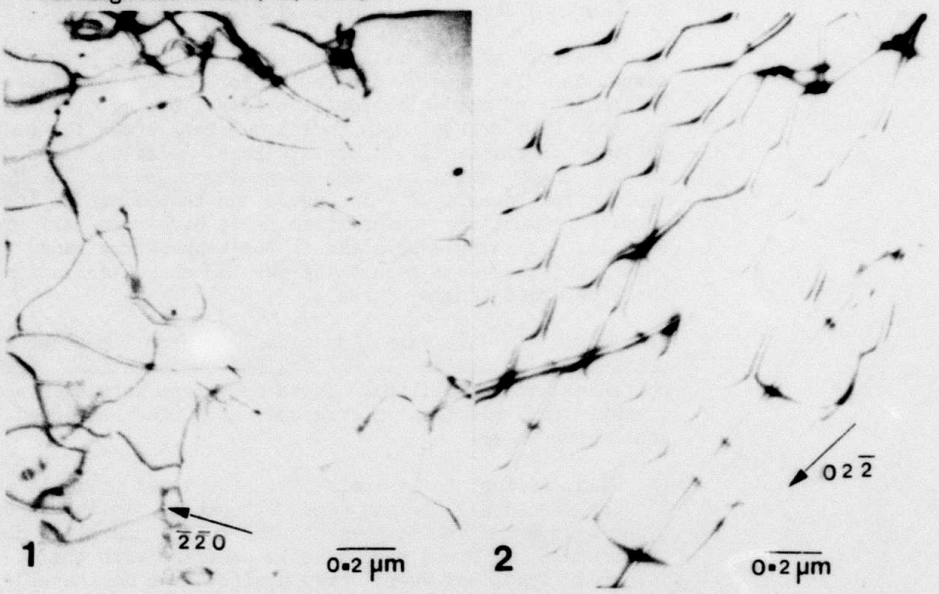

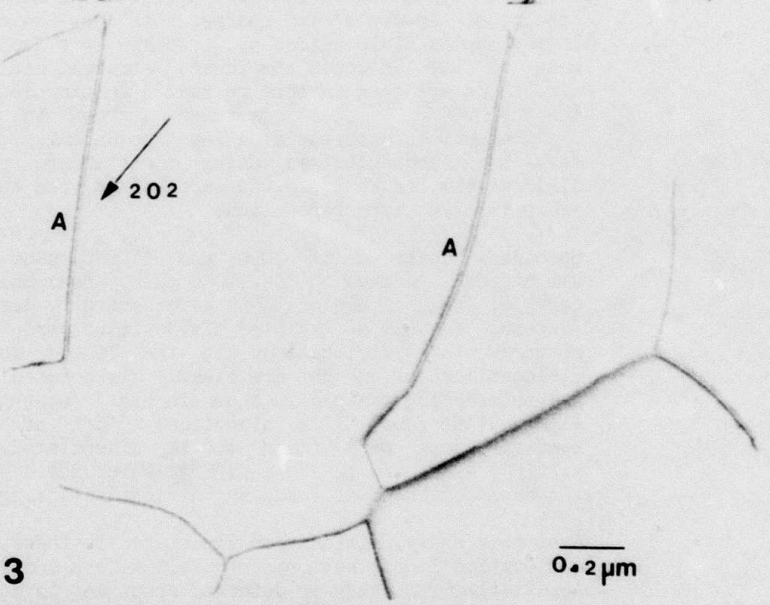

FIG. 1.--Bright field image , g[$\bar{2}\bar{2}0$], foil orientation [001].
FIG. 2.--Bright field image showing hexagonal network of dislocations, g[$02\bar{2}$], foil orientation [011].
FIG. 3.--Bright field image, g[202] and foil orientation [$\bar{1}11$].

APPENDIX C

Damage of coherent multilayer structures by injection of dislocations or cracks

J. P. Hirth
Metallurgical Engineering Department, Ohio State University, Columbus, Ohio 43210

A. G. Evans
Materials Program, College of Engineering, University of California, Santa Barbara, California 93106

(Received 24 February 1986; accepted for publication 13 June 1986)

Experimental evidence indicates that coherent multilayer structures (strained superlattices) can be grown in a damage-free state when the thickness of the layer is less than a critical value. The resistance of such structures to subsequent damage by dislocation or crack injection is examined in the present study. The structures are determined to exhibit damage resistance that decreases as either the layer thickness or the coherency strains increase.

I. INTRODUCTION

There has been burgeoning recent interest[1,2] in structures composed of alternating layers of different crystals. Of particular import are coherent, dislocation-free, multilayer structures (also called "strained superlattices"), which exhibit interesting electronic properties because of the reduced symmetry associated with the large coherency strains. However, multilayer structures can only be grown in a dislocation-free condition when the layers have thicknesses less than a critical value.[3-5] Furthermore, such structures tend to be unstable in the presence of mechanical and thermally induced stresses, particularly stresses resulting from laser irradiation.[6,7] In the present article the stability of coherent multilayer structures is analyzed with respect to injection of either dislocations or cracks. For this purpose, the residual coherency-induced stresses that exist within a multilayer system are first described. Aspects of dislocation injection in the Ga–As–P system are then evaluated. Finally, conditions for the growth of interfacial edge cracks and the decohesion of the extreme layers are estimated.

II. RESIDUAL STRESSES

Coherency between layers in a multilayer system results in residual stresses. The stresses are spatially uniform within the plane of the layer, except in the vicinity of edges. The magnitudes of the uniform stresses and the effects of edges are derived as a basis for predicting the dislocation and crack injection conditions.

A. Uniform stresses

Lattice mismatch for coherent {100} interfaces gives rise to equal biaxial stresses ($\sigma_{11} = \sigma_{22} \equiv \sigma$) and strains ($\epsilon_{11} = \epsilon_{22} = \epsilon_0$) in the two layers. For a free pair of layers, bending stresses would also be present. However, these are absent in the complete multilayer structures considered here. The boundary condition $\sigma_{33} = 0$ dictates that

$$\sigma = c\epsilon_0, \tag{1}$$

where for isotropic materials[3]

$$c = 2\mu(1+\nu)/(1-\nu),$$

with μ the shear modulus and ν Poisson's ratio; while for the anisotropic case

$$c = c_{11} + c_{12} - 2(c_{12}^2/c_{11}),$$

where c_{ij} are the elastic constants referred to the cube symmetry axes.

With reference to layers A and B (Fig. 1), mechanical equilibrium dictates that the net force on the system must be zero, whereupon,

$$\sigma_A h_A + \sigma_B h_B = 0, \tag{2}$$

where h is the layer thickness. The misfit strains must also partition such that

$$\epsilon_0 = \epsilon_A + \epsilon_B \equiv \Delta a/\langle a\rangle, \tag{3}$$

where a is the lattice parameter, $\Delta a = a_B - a_A$, and $\langle a\rangle \cong a$ (since, in all cases of interest, $\epsilon_0 < 0.01$). Combining Eqs. (1), (2), and (3) the strain at equilibrium is determined to partition according to

$$\epsilon_A = \epsilon_0 h_B c_B/(h_A c_A + h_B c_B),$$
$$\epsilon_B = \epsilon_0 h_A c_A/(h_A c_A + h_B c_B), \tag{4}$$

with the signs of ϵ_A and ϵ_B depending on the magnitudes of a_A and a_B.

B. Edge stresses

Calculation of the edge stresses induced by the coherency strain is achieved (for elastically isotropic systems) by

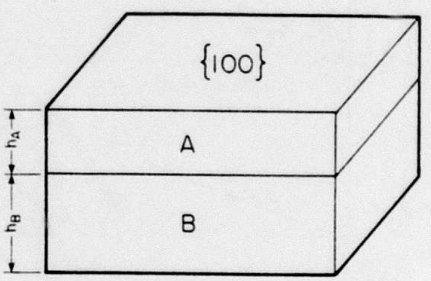

FIG. 1. A pair of layers from a multiple layer structure.

 0021-8979/86/192372-05$02.40

imposing alternating edge tractions that exactly cancel the in-plane stresses (Fig. 2). Such tractions create nonuniform stresses within the elastic half space.[8] Furthermore, the symmetry of the problem dictates that the largest localized edge stresses are the interfacial shear stresses, τ^{int}. (Note that no normal stresses exist at the central interface, at least when the elastic constants are homogeneous.) For one pair of layers, within a homogeneous semi-infinite medium, integration of the solution for a line force acting on an elastic half space[8] gives

$$\tau^{int}(2) = 2c\epsilon_0 h^2/\pi(z^2 + h^2). \tag{5}$$

The analogous result for the stress at the central interface among N pairs of such planes, is

$$\tau^{int}(N) = \frac{2c\epsilon_0 h^2}{\pi(z^2 + h^2)}\left(1 + 4z^2(h^2 + z^2) \times \sum_{n=1}^{N} \frac{(-1)^n(2n+1)}{[z^2 + (n+\frac{1}{2})^2 h^2]^2}\right). \tag{6}$$

Note that the shear stress has a maximum at the surface given by

$$\tau^{max} = 2c\epsilon_0/\pi \tag{7}$$

and becomes negligibly small at $z/h \gtrsim 4$. The peak edge shear stress is thus similar in magnitude to the uniform normal stress ($\sigma = c\epsilon_0$).

The edge stresses at the interface between the top layer and the substrate are more difficult to compute, because of the presence of the second free surface. Finite element results[9] indicate that both normal and shear stresses exist at this interface.

III. DISLOCATION INJECTION

Dislocation formation can be motivated by both the coherency and applied stresses. A lower bound estimate of the layer thickness needed to form dislocations, in the presence of these stresses, can be obtained by equating the total force on the dislocation (the Peach–Koehler force) to the line tension. This simple calculation neglects the details of the dislocation nucleation process. A more rigorous approach considers specific dislocation loop configurations at nucleation, and determines the critical nucleation condition. Both approaches are afforded brief consideration.

Dislocation formation in Ga–As–P multilayer systems has previously been considered[3] to involve the creation of a dipole on the glide plane of GaAs (Fig. 3). Alternatively, an interface dislocation may be created at the lateral surface (Fig. 4). Both configurations are examined in this article. The dipole configuration is used to illustrate the simple force balance calculation leading to the prediction of a critical layer thickness, while the interface dislocation is used to address the problem of dislocation nucleation at the lateral surface.

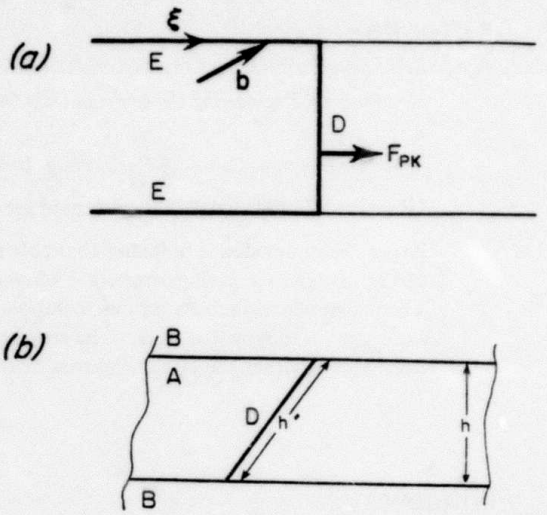

FIG. 3. View of dislocation configuration. (a) parallel to the interfaces of an A layer and perpendicular to the arms E of the dipole, (b) parallel to the interfaces of the A layer and parallel to the arms E indicating the slanted configuration of the dipole.

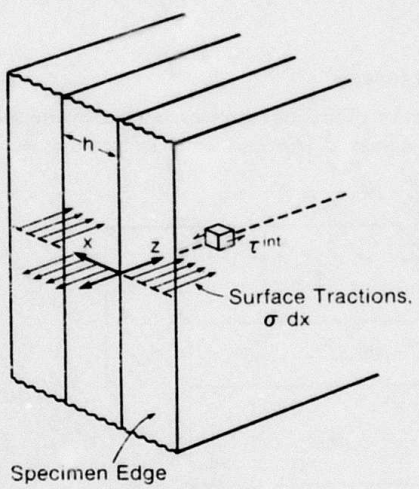

FIG. 2. Traction applied to the surface in order to evaluate the shear stress concentration σ_{12}.

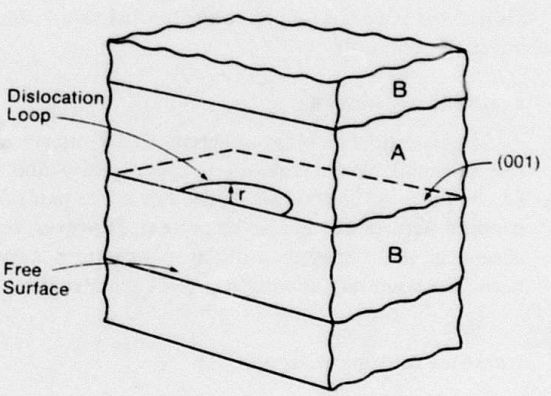

FIG. 4. Nucleation of a loop on the (001) interface.

A. The Peach–Koehler force

The force on a dislocation arising from the coherency stresses in the GaAs–$GaAs_{0.5}P_{0.5}$ system is conveniently determined in coordinates fixed on the $[001](11\bar{1})$ glide system in GaAs ($\mathbf{i}' \| [011]$, $\mathbf{j}' \| [11\bar{1}]$, $\mathbf{k}' \| [\bar{2}1\bar{1}]$). In these coordinates (Fig. 3), the Burgers vector is $\mathbf{b} = b,0,0$, the sense vector $\boldsymbol{\xi}$ is parallel to $\mathbf{k}'$ and the resolved shear stress is $(\sqrt{6}/6)\sigma$. The force on the dislocation is then the product of the force per unit length and the segment length $(\sqrt{6}/2)h$, giving

$$F_{pk} = c\epsilon_0 bh/2 \tag{8}$$

in agreement with earlier work.[3] When a stress having a shear component τ along with the slip plane is subsequently applied, the force increases, such that

$$F \equiv F_{pk} + F_a = (bh)(c\epsilon_0/2 + \sqrt{6}\tau/2). \tag{9}$$

B. Line tension force

For the configuration of Fig. 3 the line tension force on the movable segment D is

$$F_S = 2(\kappa/4\pi)\ln(\sqrt{6}h\alpha/2b), \tag{10}$$

where κ is the energy factor,[10] α is a core cutoff parameter,[11] and the factor 2 appears because two fixed segments E act on the moving segment D. In the isotropic case

$$\kappa = [\mu b^2/(1-\nu)](1 - \nu\cos^2\beta), \tag{11}$$

where β is the angle between $\mathbf{b}$ and $\boldsymbol{\xi}$. In the anisotropic case, because the Burgers vector has a screw component $b_3 = \frac{1}{4}[\bar{1}10]$ and two edge components $b_1 = \frac{1}{2}[001]$ and $b_2 = \frac{1}{4}[110]$, κ can be determined as

$$\kappa = (\kappa_1 b_1^2 + \kappa_2 b_2^2 + \kappa_3 b_3^2), \tag{12}$$

where

$$\kappa_1 = (\bar{c}'_{11} + c_{12})\left(\frac{(\bar{c}'_{11} - c_{12})c_{44}}{c'_{22}(\bar{c}'_{11} + c_{12} + 2c_{44})}\right),$$

$$\kappa_2 = (c'_{22}/c_{11})\kappa_1,$$

$$\kappa_3 = (c'_{44}c_{44})^{1/2},$$

with $c'_{22} = c_{11} + H/2$, $\bar{c}'_{11} = (c_{11}c'_{22})^{1/2}$, $c'_{44} = c_{44} - H/2$, and $H = 2c_{44} + c_{12} - c_{11}$.

C. The critical thickness

The critical layer thickness h_c, above which dislocation dipole generation becomes feasible in the absence of an applied stress, is determined by the condition $F_{pk} = F_s$. For Ga–As–P, values of this thickness are obtained using the following quantities: $\alpha = 3$, typical of compound semiconductors,[11] Voigt average values for $\mu = 48$ GPa and $\nu = 0.23$,[13] $\Delta a = 0.020$ nm and $a = 0.565$ nm for GaAs.[14] The results (Table I) are in reasonable agreement with experiment, indicating that dipole formation in GaAs does not appear to be severely nucleation limited. Moreover, the isotropic approximation gives results that do not differ drastically from those for the anisotropic approximation. It is also evident from Eq. (9) that, in the presence of an applied stress, the critical thickness is reduced to

$$h_c^+ = h_c[1 - \sqrt{6}(\tau/c\epsilon_0)]. \tag{13}$$

TABLE I. Calculated values of c, κ, and h_c.

Case	c (GPa)	κ	h_c (nm)
isotropic	153	58.5	30
anisotropic	124	57.7	39
experiment	...	...	35

D. Dislocation nucleation

Dislocation nucleation occurs most readily at the free surfaces, where image effects reduce the free energy of formation of a critical nucleus.[15] Moreover, only a small error (less than 5%) is introduced by approximating the loop as a semicircle of radius r. For an interface dislocation $\underline{b} = \frac{1}{2}[1\bar{1}0]$, forming on the (001) interface, the resolved shear stress arising from applied forces performs *work*,

$$W^a = -\pi r^2 b_1 \tau/2. \tag{14}$$

The corresponding *elastic energy* increase in the presence of a semicircular dislocation is[15]

$$U = [(2-\nu)\mu b_1^2 r/4(1-\nu)][\ln(8r\alpha/b_1) - 2] \equiv Sr, \tag{15}$$

where S is an effective line tension. However, in the presence of coherency strains, there is also an elastic energy release. The strain energy removed per dislocation is given by the product of the strain energy density and the stress relief volume. For a semicircular loop forming at the surface, the coherency contribution to the nucleus formation energy W^c can be evaluated from the edge stress [Eq. (7)] and the loop area $\pi r^2/2$, by recognizing that the zone of alternating strain has a characteristic dimension h. Then,

$$W^c \simeq (-c\pi^3\epsilon_0^2 hr^2/64) \equiv -M\pi r^2 h/2, \tag{16}$$

where $M = \pi^2 c\epsilon_0^2/32$. The total free energy accompanying loop formation is

$$\Delta G = W^a + W^c + U. \tag{17}$$

Hence, by setting $\partial\Delta G/\partial r = 0$ and applying standard nucleation theory,[15] the critical stress for dislocation nucleation τ^* becomes

$$\tau^* \equiv (S^2/40b_1kT) - (Mh/b_1) \equiv (S^2/40b_1kT)[1 - h/h^*], \tag{18}$$

where $h^* \equiv S^2/40\,MkT$ is the film thickness at which the barrier to nucleation vanishes. Typical values of τ^* for unstrained crystals[15] (0.01–0.05 μm), suggest that h^* ranges between 7 and 40 μm. Thus, h^* appreciably exceeds h_c, indicating that nucleation can represent a substantial restriction on dislocation injection. Dislocation formation at h_c thus relies upon the pre-existence of either threading dislocations or of edge loops. Furthermore, it is evident that the vulnerability to dislocation injection increases as either the misfit

strain, the layer thickness, or the imposed stress increases.

IV. CRACK FORMATION

The crack injection problem to be considered involves the formation of edge cracks between layers, caused by the concentrated coherency strains that develop in the presence of edges. The problem has some analogy with delamination cracks that initiate from edges and holes in laminated fiber composites.[16] The nature of the problem is illustrated by considering a system in which the layers have equal thickness and have the same, isotropic elastic constants.

A. The crack driving force

For elastically isotropic systems, the residual edge stresses can be used to compute stress intensity factors K for various crack configurations. Two bounding problems are presented to illustrate potential modes of cracking: interfacial edge cracks near the center of an infinite set of layers (Fig. 5) and a subsurface edge crack at the first interface (Fig. 6). For the *central edge crack*, a mode II stress intensity, K, exists, which can be determined from the stress field by use of a superposition procedure,[17]

$$K_{II} \equiv \frac{40 c\epsilon_0 h^2}{\pi^{3/2}\sqrt{a}} \int_0^a \frac{F(z/a)dz}{(z^2+h^2)\sqrt{1-(z/a)^2}}, \tag{19}$$

where $F(z/a) = [1-(z/a)^2][0.29 - 0.39(z/a)^2 + 0.77(z/a)^4 - 0.99(z/a)^6 + 0.51(z/a)^8]$ and a is the crack length. Integration of Eq. (19) gives

$$K_{II} \simeq (2.4 c\epsilon_0\sqrt{h}/\sqrt{\pi})\{(a/h)/[1+(a/h)^2]\}^{1/2}. \tag{20}$$

Trends in $K_{II}/c\epsilon_0\sqrt{h}$ with normalized crack length a/h are plotted in Fig. 5. A maximum exists at $a/h = 1$ given by

$$\hat{K}_{II} \simeq (2.4/\sqrt{2\pi}) c\epsilon_0\sqrt{h}. \tag{21}$$

Note that $K_{II} \to 0$ as a/h becomes large ($\to \infty$).

For the *subsurface edge crack*, numerical procedures are needed to determine the driving force for cracks having immediate size, $0.2 \lesssim a/h \lesssim 5$. However, for large a/h, the crack driving force may be estimated from the strain energy

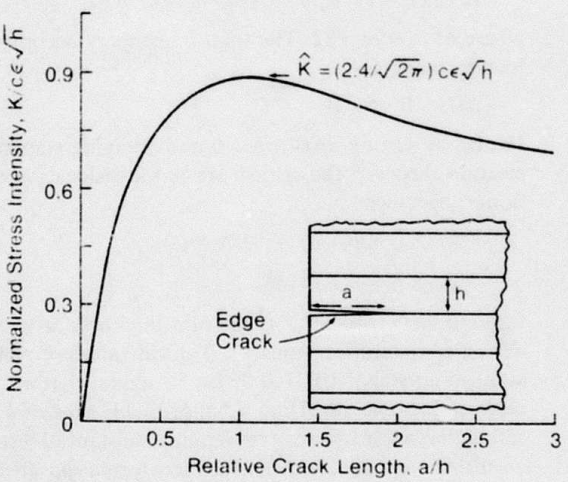

FIG. 5. Trends in normalized stress intensity factors with crack length for central edge cracks.

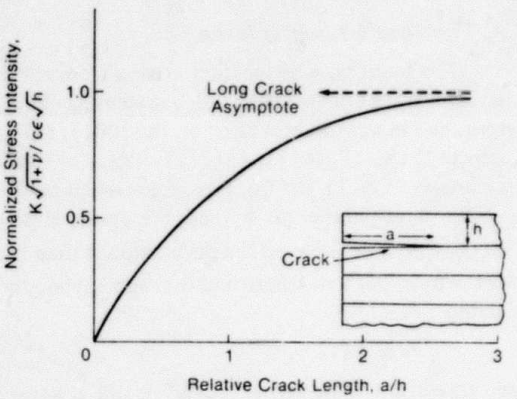

FIG. 6. Trends in stress intensity factor with crack length for subsurface edge cracks.

release in the upper layer. Specifically, the strain energy in the layer above the crack is eliminated as the crack progresses and thus constitutes a strain energy release rate. Furthermore, the strain energy concentrated around the crack tip simply advances with the crack (i.e., remains constant during crack propagation) and thus, does not contribute to the energy release rate G. Consequently, G can be deduced from the strain energy U in the layer as

$$G \equiv \frac{\partial U}{\partial a} = 2\frac{\partial}{\partial a}\frac{(c\epsilon_0)^2}{2E}(1-\nu)ha = (c\epsilon_0)^2 h(1-\nu)/E. \tag{22}$$

In view of the equivalence, $G = K^2(1-\nu^2)/E$, the effective stress intensity factor becomes

$$K/c\epsilon_0\sqrt{h} = 1/\sqrt{1+\nu}. \tag{23}$$

This analysis does not reveal whether K is single or mixed mode. However, recent calculations[18] have revealed that both mode I and mode II are involved, such that

$$K_{II}/K_I \simeq 1.4. \tag{24}$$

Evidently, Eq. (23) reveals that K is independent of crack length for large cracks. Furthermore, numerical analysis[9] reveals that K asymptotically approaches the long crack limit, as depicted in Fig. 6.

B. Crack growth

Assessment of the incidence of edge cracking requires that the crack driving force be compared with the crack growth resistance of the interface, K_c^{int} (typically in the range of 0.5–1 MPa$\sqrt{m}$ for semiconductors).[19] However, as yet, a generalized criterion for mixed mode interfacial fracture has not been determined. The simplest, reasonable postulate is that interfacial fracture occurs when $K = K_c^{int}$. By invoking Eqs. (21) and (23), one then sees that fracture may be completely averted (i.e., K never exceeds K_c^{int}) when,

$$c\epsilon_0\sqrt{h} \lesssim K_c^{int}. \tag{25}$$

Absolute assurance that the *coherency* strain does not cause

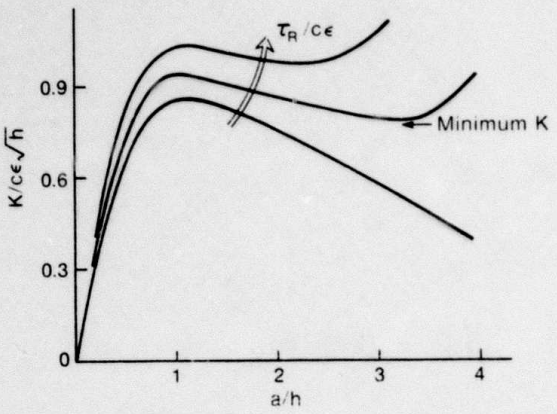

FIG. 7. The effect of applied loads τ_R on the stress intensity factor for interfacial edge cracks.

cracking thus requires that the layer thickness should not exceed a maximum value

$$h^+ = (K_c^{int}/c\epsilon_0)^2. \tag{26}$$

For the properties of Ga–As–P specified above and using $K_c^{int} \simeq 0.5$ MPa/m, h^+ is predicted as 40 nm, similar in magnitude to h_c (Table I). However, the prediction is sensitive to variations in K_c^{int}. In order to determine the specific value of layer thickness (above h_c^+) at which cracks *actually* form, independent knowledge of the magnitude of interfacial edge defects would be required. Furthermore, whereas central edge cracks would propagate inward by at most a few times the layer thickness, (because of the diminishing K_{II} at $a > h$, Fig. 6), subsurface edge cracks could cause complete separation of the top layer (Fig. 6).

When an additional *stress* is *imposed* on the structure, the cracking tendency would generally be enhanced. The details would depend on the stress distribution in the vicinity of the edges. For example, for the simple case of a uniform edge shear stress τ_R the stress intensity at central edge cracks would become

$$\frac{K_{II}}{c\epsilon_0\sqrt{h}} \approx \left(\frac{a}{h}\right)^{1/2}\left(\frac{2.4/\sqrt{\pi}}{[1+(a/h)^2]^{1/2}} + \frac{\sqrt{\pi}\tau_R}{c\epsilon_0}\right). \tag{27}$$

The normalized stress intensity is thus modified by the applied stress, as depicted in Fig. 7. Of particular interest is the minimum value of K_{II}, which essentially represents a barrier to catastrophic fracture. Specifically, when this minimum value of K_{II} exceeds K_c^{int}, complete fracture of the system becomes possible.

V. CONCLUDING REMARKS

The results presented in this article regarding dislocation injection and edge cracking in coherent layered structures, provide preliminary numerical estimates pertinent to the avoidance of deleterious damage in such structures. The estimates are independent of the overall size of the wafer, provided that the wafer diameter substantially exceeds the layer thicknesses and that many layers are involved. The results show that such structures are more vulnerable than unstrained phases, with respect to both dislocation and crack injection. The susceptibility to damage increases with increasing lattice mismatch (increasing coherency strain) and with increasing layer thickness. The present analysis of dislocation vulnerability has neglected the lattice resistance to defect motion (the Peierls stress or one of several possible pinning effects). Such factors should be important at room temperature (in Ga–As–P, for example), resulting in enhanced damage tolerance at such temperatures. However, these contributions to dislocation resistance decrease in importance with increasing temperature.

ACKNOWLEDGMENTS

This research was supported in part (J.P.H.) by the Air Force Office of Scientific Research under Grant No. F49620-85-C-0129 and in part (A.G.E.) by the Office of Naval Research under Contract No. N00014-85-K-0362.

[1] L. Esaki and R. Tsu, IBM J. Res. Dev. **14**, 686 (1970).
[2] K. Ploog and G. H. Döhler, Adv. Phys. **32**, 285 (1983).
[3] J. W. Matthews and A. E. Blakeslee, J. Cryst. Growth **27**, 118 (1974).
[4] J. W. Matthews and A. E. Blakeslee, J. Cryst. Growth **29**, 273 (1975).
[5] J. W. Matthews and A. E. Blakeslee, J. Cryst. Growth **32**, 265 (1976).
[6] N. Holonyak, Jr., R. M. Kolbas, W. D. Laidig, M. Altarelli, R. D. Dupuis, and P. D. Dapkus, Appl. Phys. Lett. **34**, 502 (1979).
[7] G. C. Osbourn, J. Appl. Phys. **53**, 1586 (1982).
[8] S. Timoshenko and J. N. Goodier, *Theory of Elasticity* (McGraw-Hill, New York, 1950).
[9] M. D. Drory and A. G. Evans, unpublished results.
[10] J. P. Hirth and J. Lothe, *Theory of Dislocations*, 2nd ed. (Wiley, New York, 1982), p. 91.
[11] J. P. Hirth and J. Lothe, *Theory of Dislocations*, 2nd ed. (Wiley, New York, 1982), p. 231.
[12] J. P. Hirth and J. Lothe, *Theory of Dislocations*, 2nd ed. (Wiley, New York, 1982), p. 453.
[13] K. Hellwege and A. M. Hellwege, *Landolt–Börnstein Tables* (Springer, Berlin, 1969), Vol. III-2.
[14] R. W. G. Wyckoff, *Crystal Structures* (Wiley, New York, 1963).
[15] J. P. Hirth, in *The Relation Between the Structure and Mechanical Properties of Metals* (H. M. Stationary Office, London, 1963), p. 217.
[16] R. B. Pipes and N. J. Pagano, J. Compos. Mater. **4**, 204 (1970).
[17] G. C. Sih, *Handbook of Stress Intensity Factors* (Lehigh University, Lehigh, PA, 1973).
[18] M. D. Thouless, A. G. Evans, M. F. Ashby, and J. W. Hutchinson (unpublished).
[19] B. R. Lawn and T. R. Wilshaw, *Fracture of Brittle Materials* (Cambridge University, Cambridge, England, 1975).